Spring 1996

# Two-Photon Quantum Interference Polarization Spectroscopy: Measurements of Transition Matrix Elements in Atomic Rubidium

Alexander I. Beger
*Old Dominion University*

# TWO-PHOTON QUANTUM INTERFERENCE POLARIZATION SPECTROSCOPY: MEASUREMENTS OF TRANSITION MATRIX ELEMENTS IN ATOMIC RUBIDIUM

by

Alexander I. Beger

M.S. May 1992, Old Dominion University

A Dissertation Submitted to the Faculty of Old Dominion University

in Partial Fulfillment of the Requirements for the Degree of

DOCTOR OF PHILOSOPHY

PHYSICS

OLD DOMINION UNIVERSITY

May, 1996

Approved by: _____
Mark D. Havey (Director)

_____

_____

_____

_____

# ABSTRACT

TWO-PHOTON QUANTUM INTERFERENCE POLARIZATION SPECTROSCOPY: MEASUREMENTS OF TRANSITION MATRIX ELEMENTS IN ATOMIC RUBIDIUM

Alexander I. Beger
Old Dominion University
Director: Dr. Mark D. Havey

The estimation of the adequacy of theoretical calculations on the atomic structure requires availability of the precise experimental data on radiative properties of the atoms. Such data is also required in astronomy and some important areas of technology. The lack of precision of traditional spectroscopic studies of atom presents a fundamental obstacle for progress in these areas. For example, in atomic rubidium, the best precision of the traditional spectroscopic results is on the order of about 1 - 5%, which does not allow for clear assessment of the latest sophisticated theoretical calculations on atomic rubidium structure, with emphasis on different, in nature, effects. This situation is typical for atomic physics in general.

The purpose of present study is obtaining the experimental data on the radiative properties of atomic rubidium with precision considerably higher than that of the traditional spectroscopic methods. This is accomplished by means of the two-photon quantum interference polarization spectroscopy. A two-photon polarization spectrum of the rubidium atom is obtained in the range of detunings -417 $cm^{-1}$ to +99 $cm^{-1}$ from atomic $5s^2S_{1/2} \rightarrow 5p^2P_{3/2} \rightarrow 8s^2S_{1/2}$ resonance. From analysis of the spectra the relativistic and many

body effects on the wavefunctions are revealed in the form of a uniquely defined parameter $q = 2\times10^{-6}$ (5) cm and an exact relation between parameters $R$ and $p$ which quantitatively describes the process:

$$R = 1.01756\ (57) + 81.466\ (15)\ p$$

where $R$ is dimensionless and $p$ is in cm. The obtained results can be thought of as specific experimentally established two-photon sum rules and can be used for testing the accuracy of the theoretical wavefunctions. The experimental technique has important advantages comparing to some traditional spectroscopic methods and is essentially free of systematic effects.

# ACKNOWLEDGMENTS

I would like to thank Dr. Mark D. Havey for guidance , help and encouragement at every stage of my research, and for many fruitful and clarifying discussions of the theoretical and technical problems associated with it. I am also thankful to my dissertation committee , Dr. Gary E. Copeland, Dr. Charles E. Hyde - Wright, Dr. Daniel E. Sonenshine, Dr. Lawrence B. Weinstein, for reading the manuscript and making useful suggestions. I express my deep appreciation to my fellow graduate students, with whom I worked at different times, especially Rodney P. Meyer for friendship and sharing his brilliant scientific talents. I thank Dr. Jacob Becher for inviting me to the wonderful field of graduate research at the Physics Department. I also thank Dr. James L. Cox for the interest in my research and help and Dr. Leposava Vušković for useful discussions and assistance with equipment. I thank Walton A. Hooks and personnel of the Machine Shop for the technical assistance. Finally I thank my family for countless sacrifices and constant support during this research.

# TABLE OF CONTENTS

# LIST OF TABLES

TABLE PAGE

# LIST OF FIGURES

FIGURE PAGE

# I. Introduction

## I.1. Preliminary remarks

The study of radiative properties of atoms is part of a general problem in physics; study of the interaction of light with matter. This relatively old problem continues to be under active research for several important reasons. These on one hand, are related to technical and theoretical problems, and on the other, to the importance of knowledge obtained in different areas of physics and technology. The complexity of the subject of investigation and of the corresponding rich variety of studies is, however, one of the primary reasons. Atoms, molecules and solids, as well as light itself and the phenomena of interaction, are represented by practically treatable and, therefore, approximate theoretical models. With the increasing precision of empirical data those models are revised from time to time. Continuing invention of new methods of analysis leads sometimes not merely to better agreement with experiment, but to better understanding of phenomena under consideration. Another reason for continuing research is that the technical problems are overcome slowly. One of the biggest technical problems is the availability of the necessary light sources. Invention of the laser, and especially those that can be frequency controlled, has revolutionized the field and stimulated

development of new experimental techniques, which continues until present time, particularly in the field of multiphoton processes. The most important, perhaps, among many reasons for continued study in the field of matter-radiation interaction is the search for new phenomena. One of the latest examples is lasing without population inversion [1]. Another challenge is more precise observation of parity nonconserving interactions in heavy atoms [2]. Spectroscopic study of such atoms, in attempts to identify and investigate parity nonconserving interactions, can prove to be an alternative to some of the usual high energy physics methods. We conclude this overview of motivating ideas by mentioning the important applications in astronomy [3] (such as determination of abundances of elements in the stars), as well as in the technology of laser isotope separation, and development of more efficient discharge lamps and plasma diagnostics.

This dissertation describes the precise measurement of some radiative properties of atomic rubidium (Rb) obtained from two-photon polarization spectra of this atom. Two-photon polarization spectra were obtained by the following procedure: atoms of Rb were promoted from their ground to the fixed excited state of the same parity by simultaneous absorption of two photons from two different tunable continuous wave lasers. The relative intensity of the subsequent fluorescence was measured as a function of the polarizations and frequencies of the absorbed photons. In this process, the sum of the frequencies of the two light sources was kept constant, thus fixing the states involved. As will be seen, a main result of the work is experimentally established two-photon matrix elements sum rules. They can serve as as a benchmark for testing

Rb atomic structure theory.

## I.2. Review of the literature

In order to understand the place of the present work among the large variety of other experiments in this area, and the motivations behind some of our choices for experimental procedure, let us make a brief review of the literature on this subject . We will consider only phenomena related to the "simplest", and in many cases most important kind of radiative transitions - electric dipole (E1). In such transitions all properties of atoms are defined by the magnitudes of electric dipole transition matrix elements, and by separation of the various atomic terms. In traditional spectroscopy the radiative properties are expressed in terms of radiative lifetimes, transition probabilities, oscillator strengths, or line strengths. These are related to one another and, under some circumstances, can be calculated from each other. Different authors often give somewhat different definitions of those quantities and in numerical comparisons special care is always required. Again, most important is that all these quantities can be expressed as some function of the electric dipole transition matrix elements. Therefore the matrix elements and relations among them can be considered as fundamental in defining radiative properties of atoms.

## I.2.1. Definition of the terms.

We start with the definition of the lifetime of an excited state of the atom. When an atom is in an excited state at some initial moment of time $t_0$, it will not stay in this state forever; eventually it will undergo a transition to a lower stable state, or to another excited state of lower energy, which will subsequently decay in a similar manner. The probability of finding the atom in the original excited state decreases exponentially with time

$$P \sim e^{-\frac{(t-t_0)}{\tau}} \qquad (1)$$

with the time constant $\tau$ being called the lifetime of the excited state. The simplicity of this concept is deceptive. The idea of spontaneous decay - as well as stimulated emission and absorption - was introduced by Einstein in 1916 [4] in an attempt to explain the Planck black body radiation law. According to B.L. Van der Waerden's characteristics [5], "All subsequent research on absorption, emission and dispersion of radiation was based on Einstein's paper (one where the idea was introduced - A.B.)". Today, eighty years later, after all the great successes of the quantum electrodynamics, the question of the physical mechanism of the spontaneous decay does not have a unique and commonly accepted answer [6].

Another quantity, related to the lifetime, is a spontaneous transition probability (so-

called Einstein A-coefficient). The quantum-mechanical expression for the spontaneous transition rate from initial $|i\rangle$ to the final $|f\rangle$ state is given, in a vacuum, by [7]:

$$A_{if} = \frac{4}{3}\frac{q^2\omega^3}{\hbar c^3}|\vec{r}_{if}|^2 \qquad (2)$$

where q is charge of the electron, $\omega$ is the energy difference between the $|i\rangle$ and $|f\rangle$ states in units of frequency, $\hbar$ is Planck's constant, c is the speed of the light and $|\vec{r}_{if}|^2$ is a square of the electric dipole transition matrix element

$$\vec{r}_{if} = \langle f|\vec{r}|i\rangle \ . \qquad (3)$$

The vector operator $\vec{r}$ represents the electron's position. Note, that if $|\vec{r}_{if}|^2$ is equal to zero (this corresponding to a so-called forbidden transition) the Einstein A-coefficient is not necessarily equal to zero. The definition must be modified in this case to describe the first nonvanishing multipole transition, for example, electric quadrupole [8]. From definitions of $A_{if}$ and $\tau$ one can see, that [9]

$$\tau_i = \frac{1}{\sum_f A_{if}} \qquad (4)$$

Thus, if a given excited state has more than one channel of decay, the measurement of its lifetime does not yield any particular transition probability, only their sum [10].

The other important quantity of the light - matter interaction is the so-called oscillator strength. The concept of oscillator strength was introduced in spectroscopy in the late

19th century [11]. At that time the electron in an atom was thought of as being elastically bound to its equilibrium position, and any sample therefore could be represented by a collection of harmonic oscillators. The electrons are also influenced by the electromagnetic field of the radiation of frequency $\omega$, which forces the atom to oscillate with the same frequency [12], inducing thereby the oscillating electric dipole moment $\vec{d}(t)$ in the sample [12]. Using this idea, the behavior of the sample can be very precisely modeled if, instead of one natural frequency of the oscillator, the number of frequencies are assumed with a fraction of oscillators $f_{ik}$ having frequency $\omega_{ik}$ . This fraction was called the oscillator strength. Comparison of the classical induced dipole moment, with the quantum-mechanical induced dipole moment shows that they are identical in form and the $f_{ik}$ value is given by

$$f_{ik} = \frac{2m_e\omega_{ik}}{3\hbar q^2}\sum_{m_i,m_k} |\langle k,m_k|q\vec{r}|i,m_i\rangle|^2 \qquad (5)$$

where "i" and "k" indicate different levels and "$m_i$" and "$m_k$" indicate (degenerate) substates of corresponding levels (usually magnetic substates).

For this reason the concept of the oscillator strength was so successful in pre-quantum spectroscopy and continues to be a useful quantity at present time. From the classical definition of the oscillator strength, it is clear that these quantities, summed over all oscillators, must yield a total number of the oscillators. In quantum mechanics the corresponding so-called sum rules were derived independently by Thomas and Kuhn in 1925 [13], and are called Thomas-Reiche-Kuhn sum rules. They are useful in many

practical calculations [14]. The last quantity we will define here is the so-called line strength. This is simply a square of electric dipole transition matrix elements, summed over all initial and final states, assuming they are degenerate. The name of this quantity reflects the fact that intensities of the spectroscopic lines, originating at a common level, are proportional to the corresponding lines strengths.

## I.2.2. Experimental methods

Experimental methods can be classified in several different ways; according to the measured quantity (lifetimes, transition probabilities, oscillator strength, line strengths), according to the process on which measurement based ( absorption, emission, anomalous dispersion, light shifts, level crossing, harmonic generation), or according to the method of excitation of the atoms and sample or light source characterization (beam-foil techniques, beam-laser techniques). During the past thirty years, nearly thirty original experimental studies on radiative properties of Rb have been reported. Review articles by C.E.Huber and R.J.Sandeman [10] and by J.Carlsson [15] have been published in 1980 and 1989 respectively.

A review of the published experimental studies, grouped according to the measured quantity, with a brief description of the method used, follows.

## I.2.2.1. Lifetimes measurements

### I.2.2.1.1 Phase-Shift method

In the phase-shift method [16] the state being studied is optically excited with intensity modulated light. The period of modulation is on the order of ten times the lifetime $\tau$ of the state under consideration. If the exciting light intensity is

$$I_{exc} = I_0 ( 1 + a \sin \Omega t ) \quad (6)$$

where $I_0$ is a base amplitude of light intensity, $I_0 a$ is the amplitude of the modulation, $\Omega$ is the angular frequency of modulation, then the intensity of the fluorescence light is [17]

$$I_{fl} = bI_0 [1 + \frac{a \sin( \Omega t + \phi )}{\sqrt{1 + \Omega^2\tau^2}}] \quad (7)$$

where $b$ is a proportionality constant and

$$\tan \phi = \Omega\tau \quad (8)$$

Measurement of $I_{fl}$ allows extraction of $\tau$. This method does not require knowledge of the sample density. Precision achieved in [16] was on the order of 2%.

## I.2.2.1.2. Level crossing

If resonance scattering takes place incoherently at two frequencies $\omega_1$ and $\omega_2$ with intensities $|f_1|^2$ and $|f_2|^2$ then the signal is proportional to

$$|f_1|^2 + |f_2|^2 \qquad (9)$$

In the case when $\omega_1$ and $\omega_2$ become equal each other - for example, under the influence of an external electric or magnetic field - the scattering becomes coherent, and the signal proportional to

$$|f_1 + f_2|^2 \qquad (10)$$

Observation of the signal in the transition from incoherent to coherent scattering is the basis for the level crossing method of lifetime measurement . The level crossing effect at zero magnetic field was first observed by W.Hanle in 1924 [18] and is referred to as the Hanle effect. A classical explanation was given at that time. In 1958 Colegrove *et al.* [19] discovered a similar effect at high magnetic field. Quantum - mechanical theory of the effect was developed by Breit in 1933 [20]. This method was used for Rb lifetime measurements in [21 - 26]. Precision achieved was on the order of 2%.

### I.2.2.1.3. Pulsed excitation and photon counting

In the pulsed excitation and photon counting method, a short ( on the order of nanoseconds) laser pulse is used to excite the atom, and subsequent fluorescent photons are detected by a photomultiplier tube. The signal exhibits exponential decay in time, which defines the lifetime of the level under consideration. This kind of the time - resolved spectroscopy gives typically 5% uncertainty [15]. The Rb excited state lifetimes obtained in [27] and [28] by this technique are in good agreement with each other except for the Rb $11s^2S_{1/2}$ level. No explanation for the discrepancy is known.

This technique is associated with serious experimental problems [15] . First of all, in the case of short lifetimes - on the same order as pulse duration - the shape of the pulse must be included in the analysis, or, alternatively, tails of the signal should be used, thus wasting most of the signal. Several problems are density related: if the atomic density must be increased ( for example, to increase the signal ) then the absorption of photons from one atom by another and subsequent reemission (radiation trapping) can artificially increase the lifetime. Also, at high densities, collisional deexcitation shortens the lifetime or changes the intensity of fluorescence in the direction of observation by depolarization of excited atoms. Therefore extreme precautions to avoid density effects must be taken and special arrangements made, such as observation at the magic angle [29] which suppresses the effects of collisional depolarization of the

fluorescence.

## I.2.2.2. Oscillator strength measurements

Out of the number of lifetime measurements discussed in the previous section, only those of the $5p^2P_{1/2,3/2}$ levels can be converted directly into transition probabilities or oscillator strengths. This is because, in the case of an excited state which has more then one channel of decay, the lifetime must be accompanied by branching ratio measurements in order to yield transition probabilities, or oscillator strengths [15]. In this section we will consider several methods of oscillator strength measurements for general excited states.

### I.2.2.2.1. The Hook method

The hook method was developed by D.S. Rozhdestvenskii in 1912 [30]. The method is based on the change of the refractive index n in the spectral region of anomalous dispersion - near an isolated absorption line. The sample, normally a metal vapor, is placed in one of the arms of a Mach-Zehnder interferometer [31]. The reference and signal beams are recombined and sent into a spectrograph. At the output, the characteristic interference picture is created in the form of "hooks", which can be photographed, or imaged electronically. By measuring the hook separation one obtains a product of the density of atoms and the oscillator strength [9]. In [32] *a posteriori* processing of

interferograms was used to enhance sensitivity and accuracy of this method. Precision ranges from 1% to 10% depending on the level considered. For normalization of the results additional information is required either in form of independently measured oscillator strengths [33] or the density of atoms [9]. Together with the lifetime of first excited state , measured by one of the methods described in the previous section, the hook method provide transition probabilities for higher excited states.

### I.2.2.2.2. Emission technique

The measured quantity in the emission technique [10,34] is the radiative energy emitted at a given frequency from a unit source volume into unit solid angle. The biggest concern is design of an "ideal" emission source: a homogeneous and stable volume of plasma. There are three direction of development in this field, these being absolute measurements, relative measurements and branching ratios. In absolute measurements the density of atoms in the excited state must be known. This constitutes a major problem for the design of sources, mainly because of the requirement of local thermodynamic equilibrium of the plasma. Typically precision is on the order of 20%.

For relative measurements the knowledge of the temperature is sufficient and therefore they are technically less difficult. They have typically precision of 10%. The results can be combined with the lifetime measurements of the first excited level to give absolute oscillator strength values. Example of this approach are found in [34], where

lifetimes from [27] where used.

Similar to this approach are experiments on branching ratios, where the "photon intensity" ratios can be measured and then combined with the lifetime of the excited states to yield absolute transition probabilities.

### I.2.2.2.3. Absorption techniques

The absorption technique is similar to the emission method, except that absorption spectra are measured. Problems of density determination required for absolute measurements are present. An important feature is that when the initial state is the ground state, the temperature determination is sufficient for absolute oscillator strength measurement ( providing that reliable vapor pressure data is available ). By this technique in [34,35,36] precision of ~10% was achieved.

### I.2.2.2.4. Third harmonic generation

The third harmonic generation method was developed by H. Puel and C.R. Vidal in 1976 [37]. Their result is often quoted but the method itself has not become commonly used. Description of the experimental procedure in [37] is rather incomplete. The method of third harmonic generation is related to the hook method because the phase-matching conditions [38] are achieved by the use of anomalous dispersion. In the quoted experiment the sample consisted of a Rb-Xe mixture with controllable partial

pressure of the components. Partial pressure was adjusted to provide the phase-matching conditions. The authors state that their experimental result for the total oscillator strength for the ground-first excited *p*-doublet ($1.07\pm.02$) is in agreement with the lifetime measurement result by R.W. Schmieder *at al.*[26]. Note that in [26] only the lifetime of the $5P_{3/2}$ level was measured ($25.5\pm.5$ns) from which only the oscillator strength ($.715\pm.014$) for the $5S_{1/2}$-$5P_{3/2}$ transition follows . Apparently the authors assumed an oscillator strength ratio for the components of the doublet to be exactly in proportion 1:2 ( whereupon the total oscillator strength is 1.073 ). In Rb, taking this ratio as 1:2 is an approximation.

### I.2.2.2.5. Inverse Hook Method

The inverse hook method was developed in 1986 by W.A.van Wijngaarden *et al.* [39,40] and is based on a light shift effect combined with polarized fluorescence measurements. It yields absolute oscillator strength between excited states of the atoms. In the experiment two pulsed lasers are used. Initially anisotropic population of the excited state sublevels is produced by absorption of two same-frequency photons . This is followed by a second light pulse of slightly different frequency than the transition under investigation. As the second pulse propagates through the metal vapor sample it does not cause any real transitions to different energy states. However, because of the so-called virtual transitions to light shifted levels, the population of excited state

sublevels changes. This is observed in the change of the polarization characteristics of the monitored fluorescence. The effect depends on the fluence of the second pulse (measured in the experiment), detuning from resonance (which is also measured) and the oscillator strength, which is a parameter of the fitting procedure.

The name "inverse hook" reflects the fact that the idea of the experiment is analogous to the one in the hook method, but the roles of atoms and radiation are inverted. In the hook method the phase of the electromagnetic wave changes as it travels through the dispersive media, while in inverse hook method, the phase of the wave function of the atom changes as it interacts with the second pulse.

The estimated uncertainty in [39,40] was 20%. This method can be applied to any excited states but it must be modified when the energy difference between the states is comparable with the half bandwidth of the interference filters used in detection of the fluorescence.

In conclusion of this rewiev one clear observation should be made: the typical precision of the considered experimental methods is currently on the order of several percent. None of them has a precision better than 1%.

## I.2.3. Theoretical methods

Detailed review of the theoretical methods in the field of radiative properties of atoms is beyond the scope of the present dissertation, which is an experimental study. A review

of earlier work can be found in [9]. Generally, many techniques to calculate atomic radiative transition properties have been developed. For example, more than 20 theoretical articles on the subject, related to Rb alone, have been published during last 20 years. The theoretical methods can be divided into groups based either on *ab initio* calculations or on effective Hamiltonian or model potential methods with adjustable semiempirical parameters. Further classification can be made based on the emphasized effect: relativistic, core polarization , core - valence electron correlation, and on approximations made and method of calculation used , such as the Hartree - Fock approach or adiabatic approximation.

The various methods provide results of varied validity, which seem best assessed by comparison with experimental compilations. The latest sophisticated calculations agree well with experiment on the level of precision 1% to 5%. To discriminate among theoretical models and methods more precise experimental data is required.

## I.3. Formulation of the problem

From the presented review of the literature it is evident, that the experimental data on radiative properties of atomic rubidium has, in the best case, the precision of about 1%. On the other hand, the estimation of the adequacy of the theoretical calculations on the atomic structure and the related radiative properties requires experimental data of considerably higher precision. Thus a gap between the need of theory and available experimental data exists.

The present work is an attempt to fill this gap. The goal of the study is to obtain more precise experimental data on atomic rubidium than that currently available from traditional spectroscopic methods, and which can be used for testing the atomic structure theory. The method used is two-photon polarization spectroscopy. As will be seen, the emphasis is made on the possibility of detection of the fine effect of the dependence of the radial wavefunction of the valence electron on its total angular momentum.

# II. Theory

The rigorous theory of two-photon absorption, as any other specific kind of radiation - matter interaction, requires application of quantum electrodynamics. Alternatively, in the semiclassical approximation [41], the radiation is considered classically and the atoms are treated quantum-mechanically. For the problem at hand the semiclassical approach provides a simpler way to account for the essential features of the process [42]. Based on this approach, the time-dependent perturbation theory was first applied to two-photon absorption by Göppert - Mayer in 1929 [43]. Certain properties of the process, particularly related to higher-order correlation functions for the two-photon excitation, require proper application of quantum electrodynamics. We will not consider them and will use the semiclassical approach. In the first part of this section the general steps in the derivation of the intensity of the two-photon absorption will be

outlined. Subsequently some features of the Rb atom, which define the process and which constitute the subject of the experimental investigation, will be considered.

# II.1. Atom - radiation interaction

The classical Hamiltonian of an atom, placed in an external electromagnetic field defined by its vector ($\vec{A}$) and scalar ($\phi$) potentials [44] can be represented as [41,45]

$$H = \frac{1}{2m}(\vec{P} - \frac{q}{c}\vec{A})^2 + V + q\phi \qquad (11)$$

where P is the linear momentum operator of the electron, V is the potential energy due to nucleus and closed shell electrons, q and m are the charge and mass of the electron, and c is speed of the light. In the Coulomb gauge [44,46]

$$\vec{\nabla} \cdot \vec{A} = 0 \, . \qquad (12)$$

The Hamiltonian can be expressed as

$$H = H_0 + W \, , \qquad (13)$$

where $H_o$ is Hamiltonian of the free atom

$$H_0 = \frac{1}{2m} P^2 + V \tag{14}$$

and W describes the interaction of the atom with the external electromagnetic wave:

$$W = \frac{q}{mc} \vec{P} \cdot \vec{A} + \frac{q^2}{2mc} A^2 \tag{15}$$

It can be shown [47], that in the electric dipole approximation [41] the interaction term is equivalent to

$$W = q\vec{r} \cdot \vec{E} \tag{16}$$

where E is the electric field of the electromagnetic wave. This form is convenient for calculations and was originally used by Göppert - Mayer [43]. The electric field in the case under consideration is a superposition of traveling wave fields from two different laser sources with frequencies $\omega_1$ and $\omega_2$ :

$$\vec{E} = \vec{E}_{01} \cos \omega_1 t + \vec{E}_{02} \cos (\omega_2 t + \alpha) \tag{17}$$

where $E_{01}$ and $E_{02}$ are corresponding vector amplitudes of the electric fields and the relative phase angle is $\alpha$.

In the following sections the transitions of the atom between stationary states caused by the time-dependent perturbation W will be considered. Some features of the unperturbed atom, which can affect the transitions and, thereby studied by two-photon polarization spectroscopy, will be described.

# II.2. Two-photon absorption

The two-photon absorption can be described in second-order time-dependent perturbation theory, as is done in several reviews on the subject and also in many nonlinear optics textbooks [9,38,42,48], or analyzed from first principles by deriving and solving the density matrix equations for the multipoles of the excited level [49]. In any case, the weak radiation field and rotating wave approximations [38] make practical calculations possible. The results can be expressed as :

$$w_{f\text{-}g} = q^4 \hbar^{-4} \Gamma_{gf}^{-1} \frac{1}{4} |E_{01}|^2 |E_{02}|^2 \times \left| \sum_n \left[ \frac{\langle f|\vec{r}\cdot\vec{e}_2|n\rangle\langle n|\vec{r}\cdot\vec{e}_1|g\rangle}{\omega_{ng}-\omega_1} + \frac{\langle f|\vec{r}\cdot\vec{e}_1|n\rangle\langle n|\vec{r}\cdot\vec{e}_2|g\rangle}{\omega_{ng}-\omega_2} \right] \right|^2 \quad (18)$$

where q is the electron charge, $\hbar$ is Planck constant, $(4\Gamma_{gf})^{-1}$ is density of final states at resonance, $\omega_{ng}$ is energy difference between the ground $|g\rangle$ and intermediate state $|n\rangle$, and $\vec{e}_i$ is a unit vector of polarization of the light from laser " i ". From this expression it is evident that the spectra of two-photon absorption is defined by the magnitude of the electric dipole matrix elements. As we will see in the next section, the matrix elements corresponding to two different intermediate states of the atom with the same principal quantum number but different total angular momentum of the electron will be different. This is not expected within the usual L-S coupling in a hydrogenic atom. Experimental observation of this difference will be described later.

# II.3. Free - atom wavefunctions

The nonrelativistic Schrödinger equation in atomic physics

$$H_0|\psi\rangle=E|\psi\rangle \qquad (19)$$

can be solved exactly only in the simplest case of hydrogen. In spherical coordinates $(r,\Theta,\varphi)$ the solution is [47] :

$$\Psi_{nlm}(r,\Theta,\varphi) = R_{nl}(r)\ Y_{lm}(\Theta,\varphi) \qquad (20)$$

where $n$ is the principal, $l$ is the orbital and $m$ is the magnetic quantum number [47]. The function $R_{nl}(r)$ can be expressed in terms of Laguerre polynomials [7,47], and the $Y_{lm}(\Theta,\varphi)$ are spherical harmonics [7,44,50]. If the spin of electron is heuristically included [47], the degeneracy of each level is $2n^2$. The degenerate wave functions can be combined in linear combinations to yield the eigenstates of the complete set of operators - energy $H_0$, orbital angular momentum $L^2$, spin angular momentum $S^2$, total angular momentum $J^2$ and one of its projections $J_z$ . The general form of such a linear combination can be written as

$$\Psi'_{nlsjm_j}(r,\Theta,\varphi) = R_{nl}(r)\ Y'_{lsjm_j}(\Theta,\varphi) \qquad (21)$$

where $Y'_{lsjmj}$ are linear combinations of the products of the spherical harmonics and the spin wavefunctions only with proper Clebsch-Gordon coefficients [51,52]. The spin-orbit interaction [47] partially removes the degeneracy and in a higher order approximation changes the radial part of the wavefunctions by mixing those with different n, but the same j. In fact, in a relativistic calculations, starting with the Dirac equation, the radial part of the wavefunction becomes explicitly dependent on the total electronic angular momentum due to the spin-orbit interaction [53]:

$$\{E + \hat{R}_1\}R_{nlj}(r)=(\hat{R}_2 + \hat{R}_3)R_{nlj}(r) \tag{22}$$

where $E$ is the energy, $R_1$ is the usual operator for the radial part of the nonrelativistic hydrogen wavefunction,

$$\hat{R}_2 = \frac{q^2\hbar^2}{4m^2c^2r^3}\,[j(j+1)-l(l+1)-s(s+1)] \tag{23}$$

and $R_3$ represents other relativistic corrections [53]:

$$\begin{aligned} \hat{R}_3 &= \hat{R}_{3a} + \hat{R}_{3b} \\ \hat{R}_{3a} &= \frac{\pi q^2\hbar^2}{2m^2c^2}\,\delta(r) \\ \hat{R}_{3b} &= -\frac{(E+\frac{q^2}{r})^2}{2mc^2} \end{aligned} \tag{24}$$

For an alkali atom like Rb, the wavefunction of the valence electron is modified by

the many-body effects, theoretically accounted for by the polarization of the core [54,55], and by correlation effects [56,57]. These effects depend on the total angular momentum of the valence electron. Therefore, in general, some dependence of the radial wavefunction on the total angular momentum is expected and according to this the total wavefunction can be written in the form

$$\Psi_{nlsjm_j}(r,\Theta,\varphi) = R_{nlj}(r)\ Y'_{lsjm_j}(\Theta,\varphi) \qquad (25)$$

Although the effect of the j-dependence of the radial part of the wavefunction is weak for low-lying levels, it can be detected in high precision experiments. These effects can become larger for large principal quantum numbers [34].

## II.4. Transition probability

Equation (18) assumes, that the atoms are at rest. In the normal experimental situation atoms are moving and, according to their velocities, they "see" Doppler shifted laser frequencies. This leads to corresponding corrections to the energy denominators in (18) and to modification of the density of the final states, which takes the form of a Lorentzian distribution for a fixed velocity group of atoms [58]. The

resulting transition probability must be integrated over the Gaussian distribution of the thermal velocities of atoms. Further complications are related to the "scanning" of one of the laser's frequency, described in section (III.4.1), and to the finite width of the frequency profile of the lasers. We will at this point make an approximation, that all mentioned effects can be taken into account by introducing the effective line shape function $\Phi(s)$ such that the transition probability can be written in the form:

$$w_{f\leftarrow g} = \Phi(s) \times \left| \sum_n \frac{\langle f|\vec{r}\cdot\vec{e}_2|n\rangle\langle n|\vec{r}\cdot\vec{e}_1|g\rangle}{\omega_{ng} - \omega_1} + \frac{\langle f|\vec{r}\cdot\vec{e}_1|n\rangle\langle n|\vec{r}\cdot\vec{e}_2|g\rangle}{\omega_{ng} - \omega_2} \right|^2 \qquad (26)$$

where "s" stands for all variables describing Doppler broadening, laser lineshapes and "scanning" effects. Equation (26) particularly applies to two-photon transitions and it requires careful examination. Obviously, if all transition matrix elements and frequencies are known, then, in principle, for any resonant combination of $\omega_1$ and $\omega_2$, the series in (26) can be explicitly evaluated yielding the transition probability. Usually the frequencies are known experimentally to a high precision [59], or can be accurately calculated using quantum-defect theory [60]. In contrarast to this, the wavefunctions, and thus the matrix elements, are not very well known [10]. One then faces a question: is it possible to perform a high precision experimental measurement of a transition probability, or some related quantity, such that precise values of the matrix elements (or some simple functions of them) can be extracted. If possible, such an experiment can serve as a benchmark for testing atomic structure theory. The present research is an attempt to answer this question. As will be shown later, the answer is

positive.

A quick solution, which equation (26) suggests, is to make a particular denominator so small that the corresponding term will dominate all other contributions and, in an appropriate limit, make them negligible. Then the transition probability will become a direct measure of the corresponding product of matrix elements. This way, also possible in principle, is not an appropriate one for high precision measurements. First of all, the lineshape function $\Phi(s)$ is difficult to precisely estimate. Secondly, one will necessary run into the problem of light shifts [61], and possibly, real population of the intermediate level(s) and the associated problems of single photon spectroscopy (see Introduction).

If the number of the terms in (26) was finite (N), then with appropriate choice of polarization one could measure the transition probability at ~ 2N different combinations of frequencies and obtain values of the products of matrix elements. Note that the "2" is related to the fact, that (26) is a quadratic form. This approach, however, is not practical, because the number of terms in (26), is infinite. Alternatively, one can try to determine experimentally such combinations of the frequencies $\omega_1$ and $\omega_2$ that the transition probability (26) is zero. The structure of (26) suggests, that there will be ~N such roots, corresponding to total destructive interference among contributions from intermediate levels, which in general correspond to fine, or even hyperfine, structure of the atom. If such roots are found experimentally with high precision, they represent exact information about atomic structure and can be used to test atomic structure theory. For finite N they can give a system of linear equations to yield all N products

of matrix elements. For infinite N some practical approximations can be made. In the following sections we will consider a specific example of this approach in the case of Rb, where one root is located between the frequencies of the $5s^2S_{1/2} \rightarrow 5p^2P_{1/2}$ and $5s^2S_{1/2} \rightarrow 5p^2P_{3/2}$ transitions. It is important to note that because the multiplet separations, fine structure splitting and natural lifetime of each intermediate p-level has a scaling on effective principal quantum number of $(n^*)^{-3}$ [60], a similar description is expected to be repeated at each value of $n^*$.

## II.5. Application to Rubidium.

If now the states $|g>$, $|n>$ and $|f>$ are taken in the form (25), the angular part of the matrix elements can be simply evaluated, providing that all operators are presented in irreducible tensor form, and the Wigner-Eckart theorem is used [51]. Specifically, for an experimental geometry with two laser beams traveling in the same direction and having the same direction of polarization and for the $5s^2S_{1/2} \rightarrow 8s^2S_{1/2}$ two-photon transition in Rb the only contributing intermediate states are $np^2P_j$ levels ($j=1/2;3/2$) with $n=5,6,\ldots$ . The result is

$$w^{\parallel}_{8S-5S} \equiv I_{\parallel} = \Phi(s) \times \left| \sum_{n\geq 5} \left[ \frac{2\langle 8S_{1/2}\| r \|nP_{3/2}\rangle\langle nP_{3/2}\| r \|5S_{1/2}\rangle}{\omega_1 - (\omega_{np_{3/2}} - \omega_{5S})} + \frac{\langle 8S_{1/2}\| r \|nP_{1/2}\rangle\langle nP_{1/2}\| r \|5S_{1/2}\rangle}{\omega_1 - (\omega_{np_{1/2}} - \omega_{5S})} + \frac{2\langle 8S_{1/2}\| r \|nP_{3/2}\rangle\langle nP_{3/2}\| r \|5S_{1/2}\rangle}{\omega_2 - (\omega_{np_{3/2}} - \omega_{5S})} + \frac{\langle 8S_{1/2}\| r \|nP_{1/2}\rangle\langle nP_{1/2}\| r \|5S_{1/2}\rangle}{\omega_2 - (\omega_{np_{1/2}} - \omega_{5S})} \right] \right|^2 \quad (27)$$

But if the direction of polarization of one of the beams is rotated from its direction in the previous configuration by $\pi/2$ about the axis of propagation, and all other conditions kept the same, the result for two-photon absorption becomes:

$$w^{\perp}_{8S-5S} \equiv I_{\perp} = \Phi(s) \times \left| \sum_{n\geq 5} \left[ \frac{\langle 8S_{1/2}\| r \|nP_{3/2}\rangle\langle nP_{3/2}\| r \|5S_{1/2}\rangle}{\omega_1 - (\omega_{np_{3/2}} - \omega_{5S})} - \frac{\langle 8S_{1/2}\| r \|nP_{1/2}\rangle\langle nP_{1/2}\| r \|5S_{1/2}\rangle}{\omega_1 - (\omega_{np_{1/2}} - \omega_{5S})} - \frac{\langle 8S_{1/2}\| r \|nP_{3/2}\rangle\langle nP_{3/2}\| r \|5S_{1/2}\rangle}{\omega_2 - (\omega_{np_{3/2}} - \omega_{5S})} + \frac{\langle 8S_{1/2}\| r \|nP_{1/2}\rangle\langle nP_{1/2}\| r \|5S_{1/2}\rangle}{\omega_2 - (\omega_{np_{1/2}} - \omega_{5S})} \right] \right|^2 \quad (28)$$

The so-called reduced matrix elements in equations (27) and (28) are defined by the following radial integrals:

$$\langle nlj \| r \| n'l'j' \rangle = \int_0^\infty R^*_{nlj} R_{n'l'j'} r^3 dr \qquad (29)$$

The dependence of the $R_{nlj}$ on the total angular momentum j is seen now as one of the factors defining intensities of two-photon absorptions. In the following sections the possibility of the experimental observation of this dependence will be considered. But first let us consider possible effects of the hyperfine structure of rubidium.

## II.6. Hyperfine structure and isotope shifts effects.

The sample in the experiment consisted of the naturally occurring Rubidium isotopes: $^{85}$Rb and $^{87}$Rb. The isotope $^{85}$Rb has nuclear spin of 5/2 and is stable. The isotope $^{87}$Rb has nuclear spin of 3/2 and is slightly radioactive with a half - life on the order of $10^{11}$ years. The relative abundance of this isotope is 27.85% [62]. The electronic properties of different isotopes are different, because of the electromagnetic interaction of the electrons with nuclear moments [63,64]. The detailed analysis of the effects involved in the hyperfine interactions is outside the scope of the present work and can be found elsewhere [64]. We will consider only the effects most directly related to our study: the hyperfine splitting of the levels participating in the transitions, their isotope shifts and the two-photon transition probabilities between hyperfine structure components.

The location of the hyperfine energy levels is given by the following expression [64]:

$$W_F = \frac{1}{2}hAK + hB\frac{\frac{3}{2}K(K+1)-2I(I+1)J(J+1)}{2I(2I-1)2J(2J-1)} \quad (30)$$

where A is the magnetic dipole coupling constant, B is the electric quadrupole coupling constant, I is the nuclear spin, J is the total angular momentum of the electron and K is defined by [64]:

$$K = F(F+1)-I(I+1)-J(J+1) \quad (31)$$

where F is the quantum number representing the total angular momentum of the atom:

$$\vec{F} = \vec{J} + \vec{I} \quad (32)$$

Note that the quadrupole interaction is present only for I,J $\geq 1$ and that in the s-states the magnetic dipole interaction is determined only by the contact interaction [64]. The hyperfine splittings obtained with numerical data from [64] are summarized in Fig.1. The isotope shift for the $5s^2S_{1/2}$-$8s^2S_{1/2}$ transition ($145 \pm 40$MHz) was quoted in [65]. We have calculated expressions for the two-photon transition probabilities between any pair of the ground and excited level's hyperfine components. The results of simple, but tedious calculations can be conveniently summarized in the form of diagrams, similar to the Kastler diagrams [66], Fig.2. The diagrams have the following meaning: the arrows indicate allowed transitions (under the given conditions of direction of polarization and resonance), while the numbers indicate the relative intensity of the given

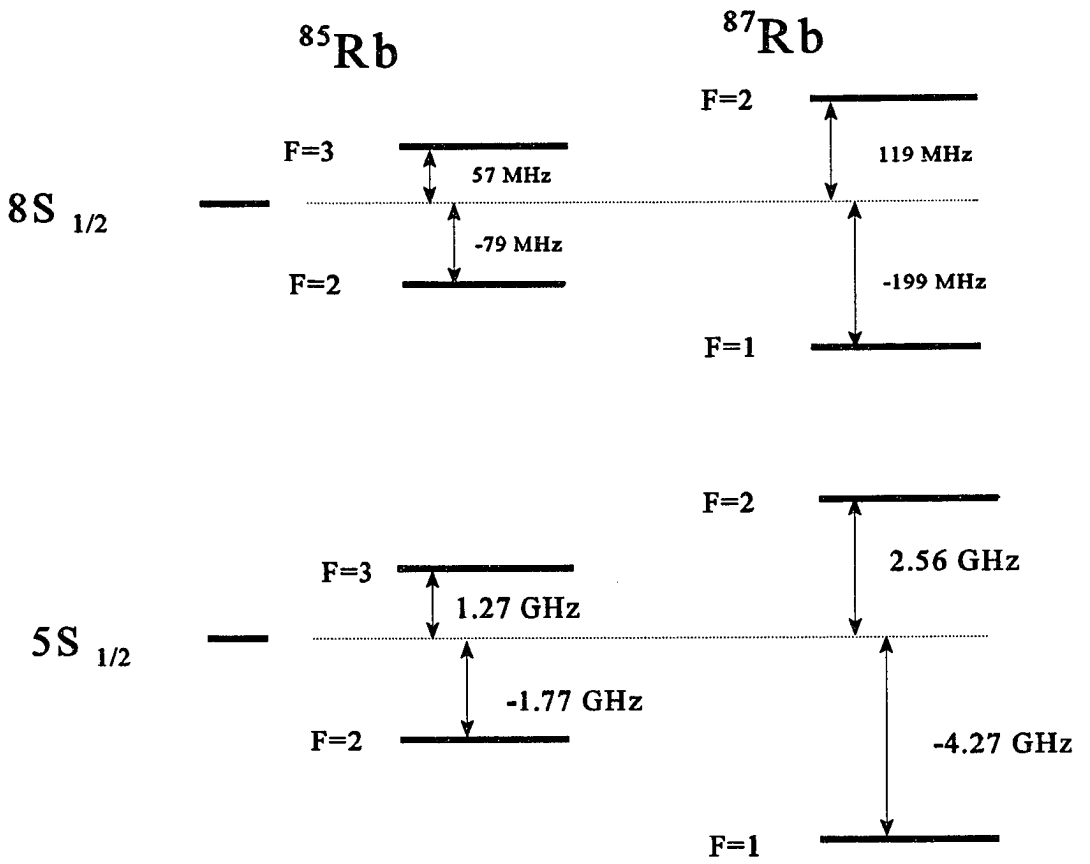


Figure 1. Hyperfine structure of rubidium.

# $^{87}Rb$ , I = 3/2

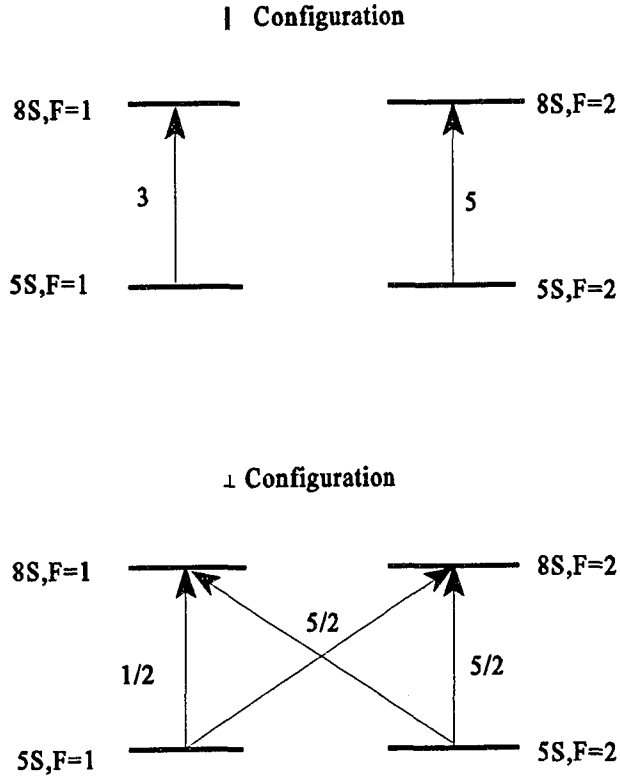


Figure 2. Transitions between hyperfine structure components. Isotope $^{87}Rb$.

transition. Thus, in the case of mutually perpendicular directions of polarization of two laser beams, the transitions $5s^2S_{1/2}(F=2) \rightarrow 8s^2S_{1/2}(F=2)$ and $5s^2S_{1/2}(F=2) \rightarrow 8s^2S_{1/2}(F=1)$ are possible with the same relative intensity 5/2. We point out, that the part of the general selection rules $\Delta F = \pm 1$, is not always realized [67].

The averaging over the hyperfine structure of the intermediate states makes calculations much more concise [66,b] and yields the same result. This approach was used to calculate effects of hyperfine interactions in $^{85}Rb$ (I=5/2) [66,b]. The results are represented in Fig.3.

The obtained results indicate that the hyperfine interactions, under excitation with completely resolved hyperfine structure, would considerably modify the polarization spectra. Experimental verification will require lasers much more narrow than those we are presently using. Averaging over all hyperfine components has zero net result on the electronic polarization spectrum obtained earlier, as expected.

## II.7. Numerical estimations

From equations (27) and (28) one can see that by appropriate choice of $\omega_1$ and $\omega_2$ some terms in the sums can be enhanced and others suppressed. For example, if $\omega_1$ is chosen within several hundred $cm^{-1}$ from the one-photon transition $5s^2S_{1/2} \rightarrow 5p^2P_{1/2}$ or $5s^2S_{1/2} \rightarrow 5p^2P_{3/2}$ ( the so-called $D_1$ or $D_2$ lines respectively ), then the contributions

# $^{85}Rb$ , I=5/2

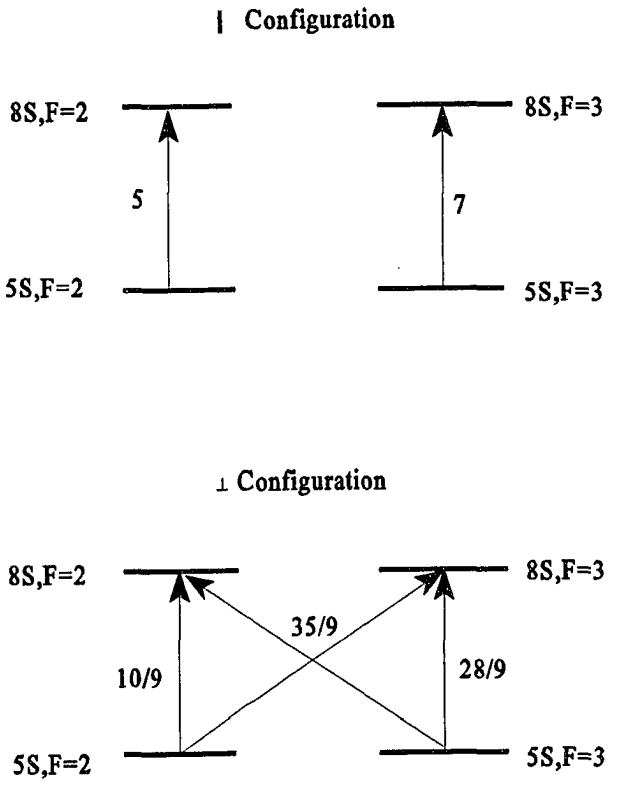


Figure 3. Transitions between hyperfine structure components. Isotope $^{85}Rb$.

from intermediate $5p^2P_{1/2}$ and $5p^2P_{3/2}$ states will dominate all other contributions (see energy level diagram of Rb, Fig.(8) ). In such case the equations (27) and (28) can be rewritten as

$$I_{\parallel}=\Phi(s)\times\left| \frac{2\langle 8S_{1/2}\| r \|5P_{3/2}\rangle\langle 5P_{3/2}\| r \|5S_{1/2}\rangle}{\omega_1-(\omega_{5p_{3/2}}-\omega_{5S})} + \frac{\langle 8S_{1/2}\| r \|5P_{1/2}\rangle\langle 5P_{1/2}\| r \|5S_{1/2}\rangle}{\omega_1-(\omega_{5p_{1/2}}-\omega_{5S})} \right.$$
$$\left. + \frac{2\langle 8S_{1/2}\| r \|5P_{3/2}\rangle\langle 5P_{3/2}\| r \|5S_{1/2}\rangle}{\omega_2-(\omega_{5p_{3/2}}-\omega_{5S})} + \frac{\langle 8S_{1/2}\| r \|5P_{1/2}\rangle\langle 5P_{1/2}\| r \|5S_{1/2}\rangle}{\omega_2-(\omega_{5p_{1/2}}-\omega_{5S})} + p' \right|^2 \quad (33)$$

$$I_{\perp}=\Phi(s)\times\left| \frac{\langle 8S_{1/2}\| r \|5P_{3/2}\rangle\langle 5P_{3/2}\| r \|5S_{1/2}\rangle}{\omega_1-(\omega_{5p_{3/2}}-\omega_{5S})} - \frac{\langle 8S_{1/2}\| r \|5P_{1/2}\rangle\langle 5P_{1/2}\| r \|5S_{1/2}\rangle}{\omega_1-(\omega_{5p_{1/2}}-\omega_{5S})} \right.$$
$$\left. - \frac{\langle 8S_{1/2}\| r \|5P_{3/2}\rangle\langle 5P_{3/2}\| r \|5S_{1/2}\rangle}{\omega_2-(\omega_{5p_{3/2}}-\omega_{5S})} + \frac{\langle 8S_{1/2}\| r \|5P_{1/2}\rangle\langle 5P_{1/2}\| r \|5S_{1/2}\rangle}{\omega_2-(\omega_{5p_{1/2}}-\omega_{5S})} + q' \right|^2 \quad (34)$$

where p′and q′ include contributions of all intermediate states $np^2P_j$ with $n>5$, with the corresponding intensities. The normalized difference of $I_{\perp}$ and $I_{\parallel}$ , called a linear polarization degree

$$P_L=\frac{I_{\parallel}-I_{\perp}}{I_{\parallel}+I_{\perp}} \quad (35)$$

can be conveniently measured in experiment (this will be discussed later). In the expressions for the intensities $I_{\perp}$ and $I_{\parallel}$ used for theoretical evaluation of $P_L$, the line-shape function $\Phi(s)$ does not, under appropriate circumstances, effect $P_L$ , and can be dropped. Also, it is convenient to denote the ratio of the combinations of the reduced

matrix elements, due to the $5p^2P_{3/2}$ and the $5p^2P_{1/2}$, by $R$,where

$$R \equiv \frac{\langle 8S_{1/2}\| r \|5P_{3/2}\rangle\langle 5P_{3/2}\| r \|5S_{1/2}\rangle}{\langle 8S_{1/2}\| r \|5P_{1/2}\rangle\langle 5P_{1/2}\| r \|5S_{1/2}\rangle}, \tag{36}$$

the difference of the frequency of laser 1 and the resonance $5s^2S_{1/2}\rightarrow 5p^2P_{3/2}$ frequency by $\Delta$, where

$$\Delta \equiv \omega_1 - (\omega_{5P_{3/2}} - \omega_{5S_{1/2}}), \tag{37}$$

and the auxiliary frequency differences as

$$\begin{aligned} d_{fs} &= \omega_{5P_{3/2}} - \omega_{5P_{1/2}}, \\ D &= \omega_{8S_{1/2}} - \omega_{5S_{1/2}} - 2\,\omega_{5P_{3/2}}. \end{aligned} \tag{38}$$

With these notations the intensities (33) and (34) can be rewritten as follows:

$$I_{\|} = \left[ \frac{2R}{\Delta} + \frac{1}{d_{fs} + \Delta} + \frac{2R}{D - \Delta} + \frac{1}{D + d_{fs} - \Delta} + p \right]^2, \tag{39}$$

$$I_{\perp} = \left[ \frac{R}{\Delta} - \frac{1}{d_{fs} + \Delta} - \frac{R}{D - \Delta} + \frac{1}{D + d_{fs} - \Delta} + q \right]^2, \tag{40}$$

where

$$p = \frac{p'}{\langle 8S_{1/2}\| r \|5P_{1/2}\rangle\langle 5P_{1/2}\| r \|5S_{1/2}\rangle}, \tag{41}$$

$$q = \frac{q'}{<8S_{1/2}\| r \|5P_{1/2}><5P_{1/2}\| r \|5S_{1/2}>} , \tag{42}$$

and the use of the two-photon resonance condition

$$\omega_1 + \omega_2 = \omega_{8S_{1/2}} - \omega_{5S_{1/2}} \tag{43}$$

have been made. Note that numerically [59,62]

$$\begin{aligned} d_{fs} &= 237.60\ (\ 1\ )\ cm^{-1}\ , \\ D &= 3413.72\ (\ 3\ )\ cm^{-1}\ . \end{aligned} \tag{44}$$

If now the variable Δ, called detuning, is varied in the range ~500 $cm^{-1}$ , the magnitudes of $p$ and $q$ remain to a good approximation independent of Δ. The variation of $P_L$ as a function of Δ will depend parametrically on $R$, $p$ and $q$ and, as we will see, will define $q$ and establish a functional relationship between $R$ and $p$. This experimentally established relation, combined with relatively low precision estimation of p, can yield a value of r with precision on the order of 0.1%. Thus the fine effect of j-dependence of the radial wave function can by this procedure be measured with unusually high precision (when compared to the precision quoted in the review of experimental methods).

# III. Experiment

This section describes the experimental part of the research, starting with preparing the sample and assembling the experimental device components and concluding with acquiring the data and storing the information.

## III.1. General characteristics of the experiment

The essence of the experiment is illustrated in Fig.4. Two nearly parallel laser beams, traveling in the y-direction of the coordinate system, enter the Pyrex cylindrical cell containing rubidium vapor. The beams are tightly focused at the approximate geometrical center of the cell, point O, chosen to be the center of the coordinate system. The two-photon absorption takes place predominantly in a small volume around point O, called the interaction region. The subsequent fluorescence from rubidium atoms in the interaction region is detected by a photomultiplier tube, positioned on the x- axis, through a system of windows. The polarization direction of one of the beams is permanently fixed in the direction of the z-axis. The polarization direction of the other beam is changed periodically from the z direction to the x direction and back ( for ~100 times in a typical experimental run). The fluorescence photons, detected by the photomultiplier tube, are counted by a computerized photon counting system. These numbers, one for the configuration with parallel relative beam

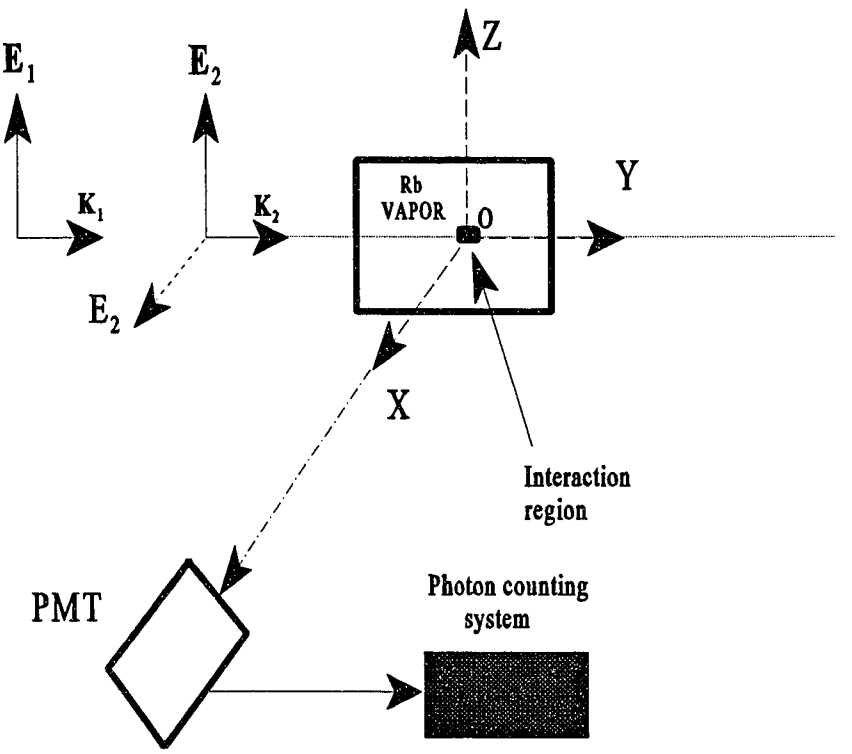


Figure 4. General experimental setup for polarization degree measurements.

polarization ($N_{\|}$) and one for the perpendicular relative beam polarization ($N_{\perp}$) are combined to yield a polarization degree:

$$P_L = \frac{N_{\|} - N_{\perp}}{N_{\|} + N_{\perp}} . \tag{45}$$

This expression, of course, is just an experimental counterpart to the theoretical polarization degree, defined by equation (35).

The two-photon absorption process can be represented by a convenient mnemonic picture based on the energy diagram of the atom, as shown in the following discussion. Consider again the two-photon transition probability, eq.(26). The general term of the infinite summation over the set of the intermediate states $|n\rangle$ consist of two parts. One of them, namely

$$\frac{\langle f|\vec{r}\cdot\vec{e}_2|n\rangle\langle n|\vec{r}\cdot\vec{e}_1|g\rangle}{\omega_{ng} - \omega_1} \tag{46}$$

represent the amplitude of the following process: a photon from laser 1 promotes the atom from the ground state $|g\rangle$ to an intermediate state $|n\rangle$, then a photon from laser 2 promotes the atom from $|n\rangle$ to the final state $|f\rangle$. Note, that this process is not a real one in the sense that no atom actually appears in the intermediate state, as it would contradict the conservation of the energy principle. These sorts of process, called virtual processes, are however, elements of the reality of the quantum world, where they contribute the interfering probability amplitudes to the "actual" process of the

transition of the atom from the initial (ground) to the final (excited) state. In the case under consideration, the only contributing intermediate states are $|nP_j\rangle$ (n=5,6,...; j=1/2, 3/2) and the virtual process can be depicted schematically on the energy diagram of rubidium as shown on Fig.5.

Alternatively, the infinite set of the virtual process can be represented by one two-step transition via a virtual level of the atom, the position of which is higher than the energy of the ground level by the energy of the first photon, as shown in Fig.6.

The analogous consideration of the other general term in eq.(26),

$$\frac{\langle f|\vec{r}\cdot\vec{e}_1|n\rangle\langle n|\vec{r}\cdot\vec{e}_2|g\rangle}{\omega_{ng}-\omega_2} \qquad (47)$$

where the roles of the photons 1 and 2 are interchanged, in comparing to (46), leads to a pictorial representation, shown in Fig.7. Combining pictures from Fig.6 and Fig.7, the final picture of the two-photon process features two virtual intermediate levels of the atom, as shown in Fig.8.

# III.2. Geometry of the experiment

The geometry of the experiment is shown in Fig.9. The following is a short overview of the arrangement of experimental components. These are individually described in more detail in the following sections. A Coherent $Ar^+$ ion laser, Model Innova 70-4,

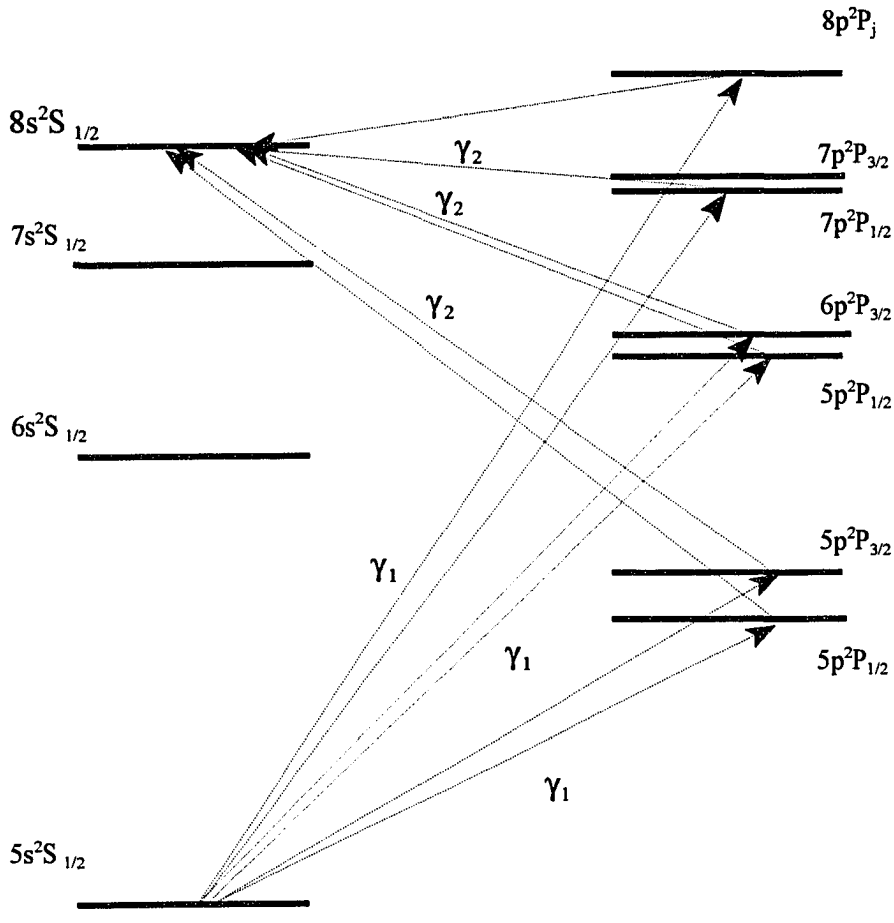


Figure 5. Virtual transitions from the initial (ground) $5s^2S_{1/2}$ level to the final (excited) $8s^2S_{1/2}$ level via the intermediate $np^2P_j$ levels. The first step is caused by the photon from the source 1; second - by the photon from the source 2.

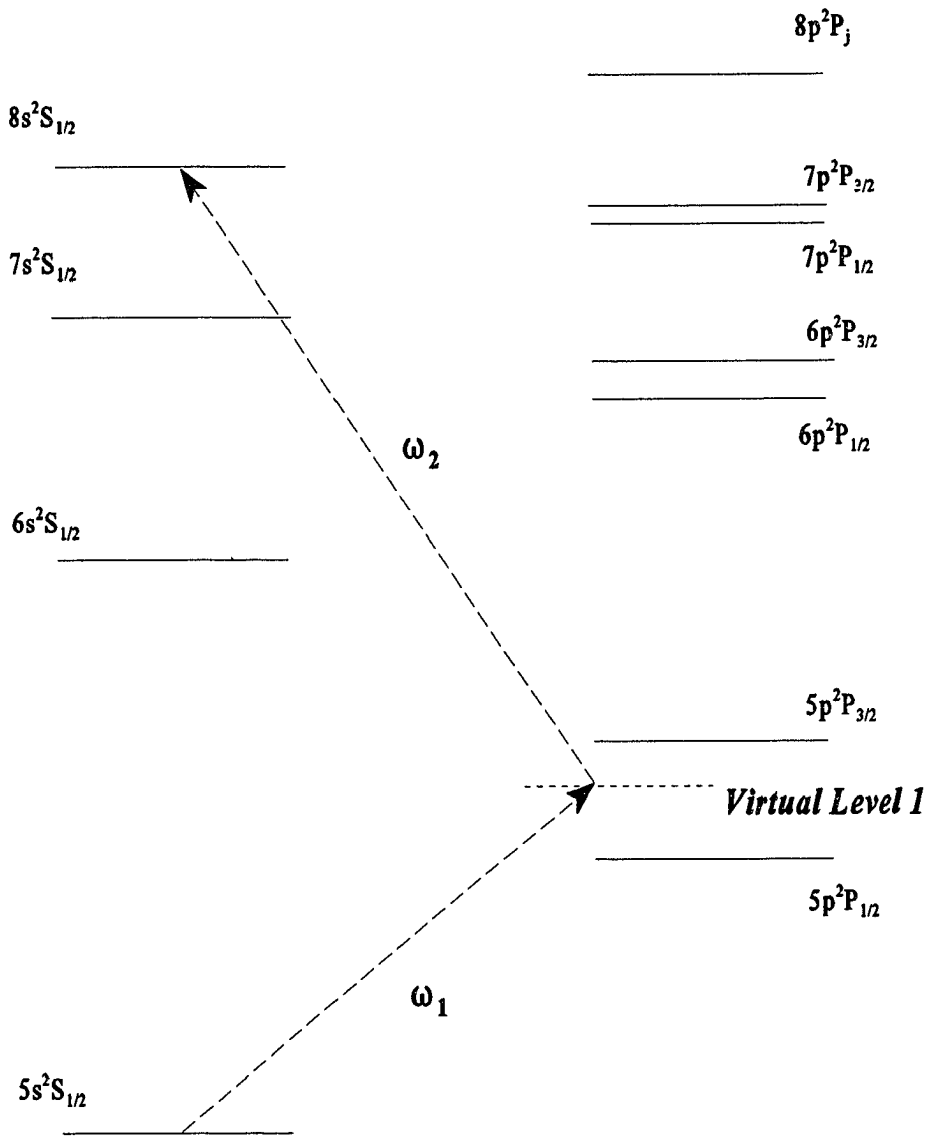


Figure 6. The alternative graphic representation of the virtual transitions via the virtual level 1.

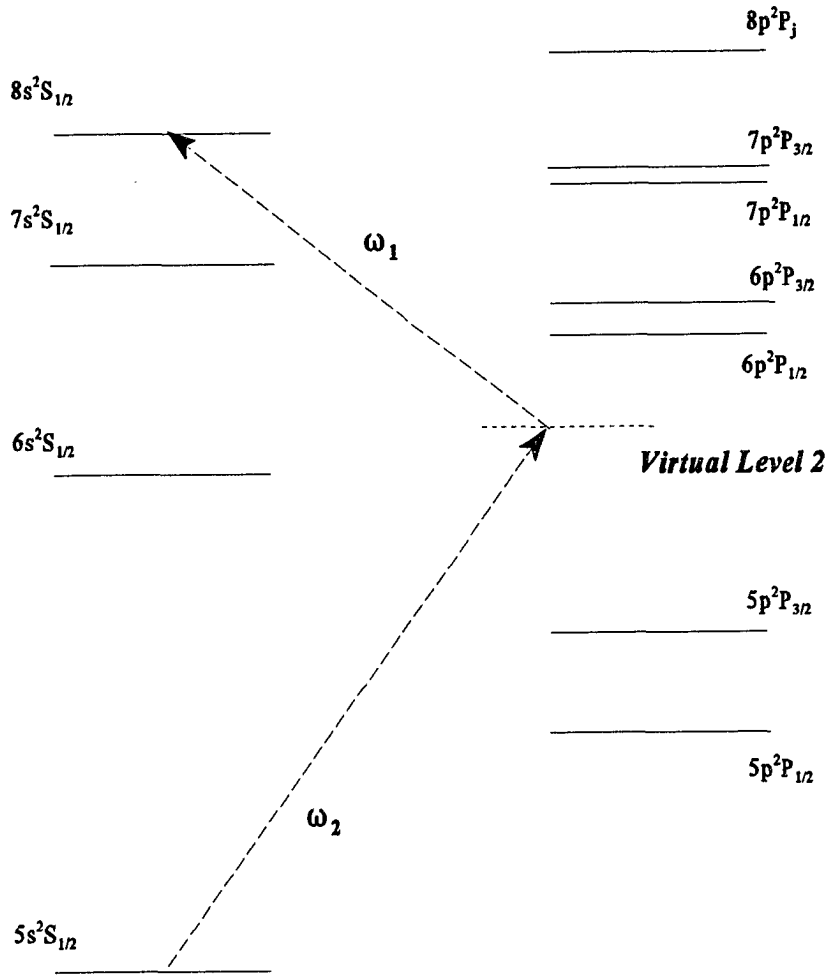


Figure 7. The alternative graphic representation of the virtual transitions via the virtual level 2.

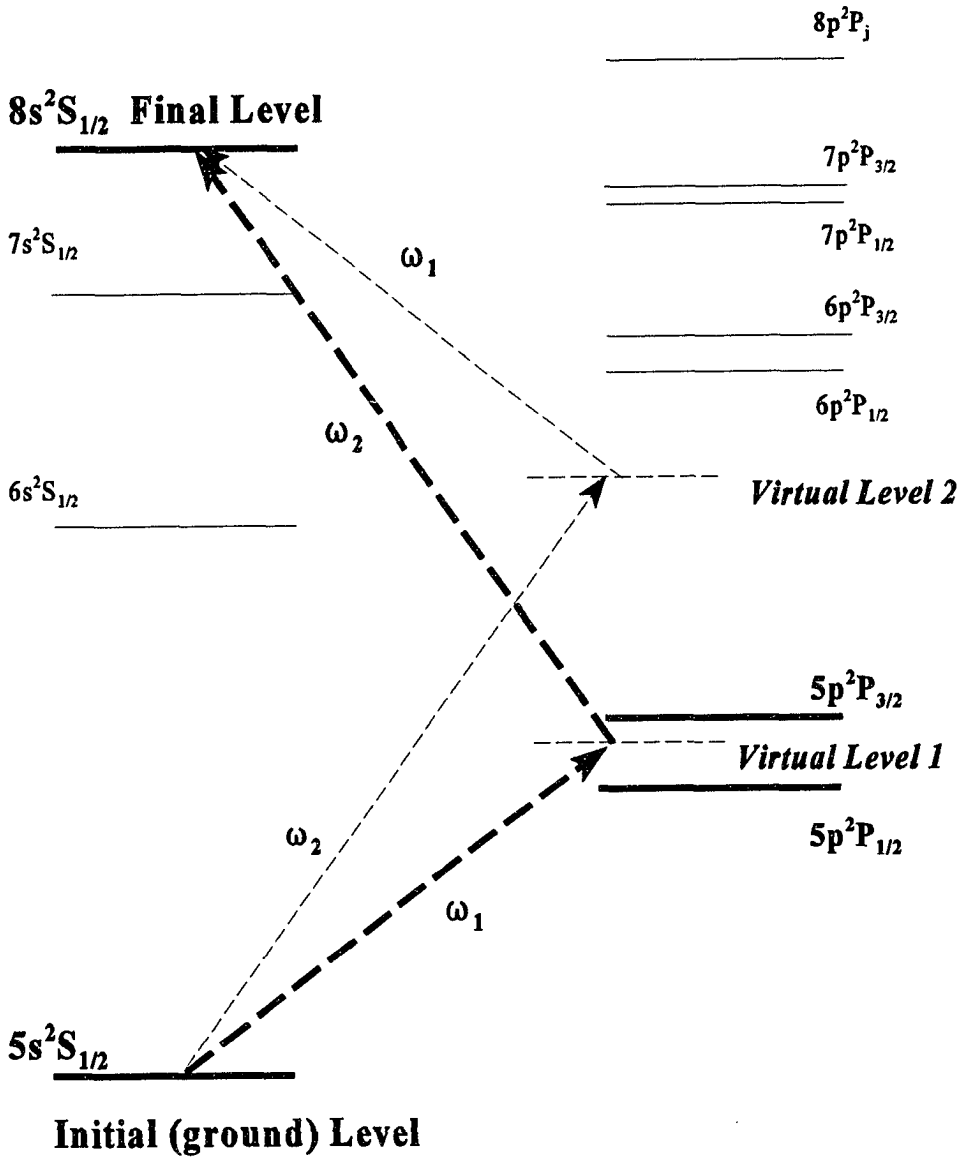


Figure 8. The graphic representation of the prosess of the two-photon absorption via two virtual levels.

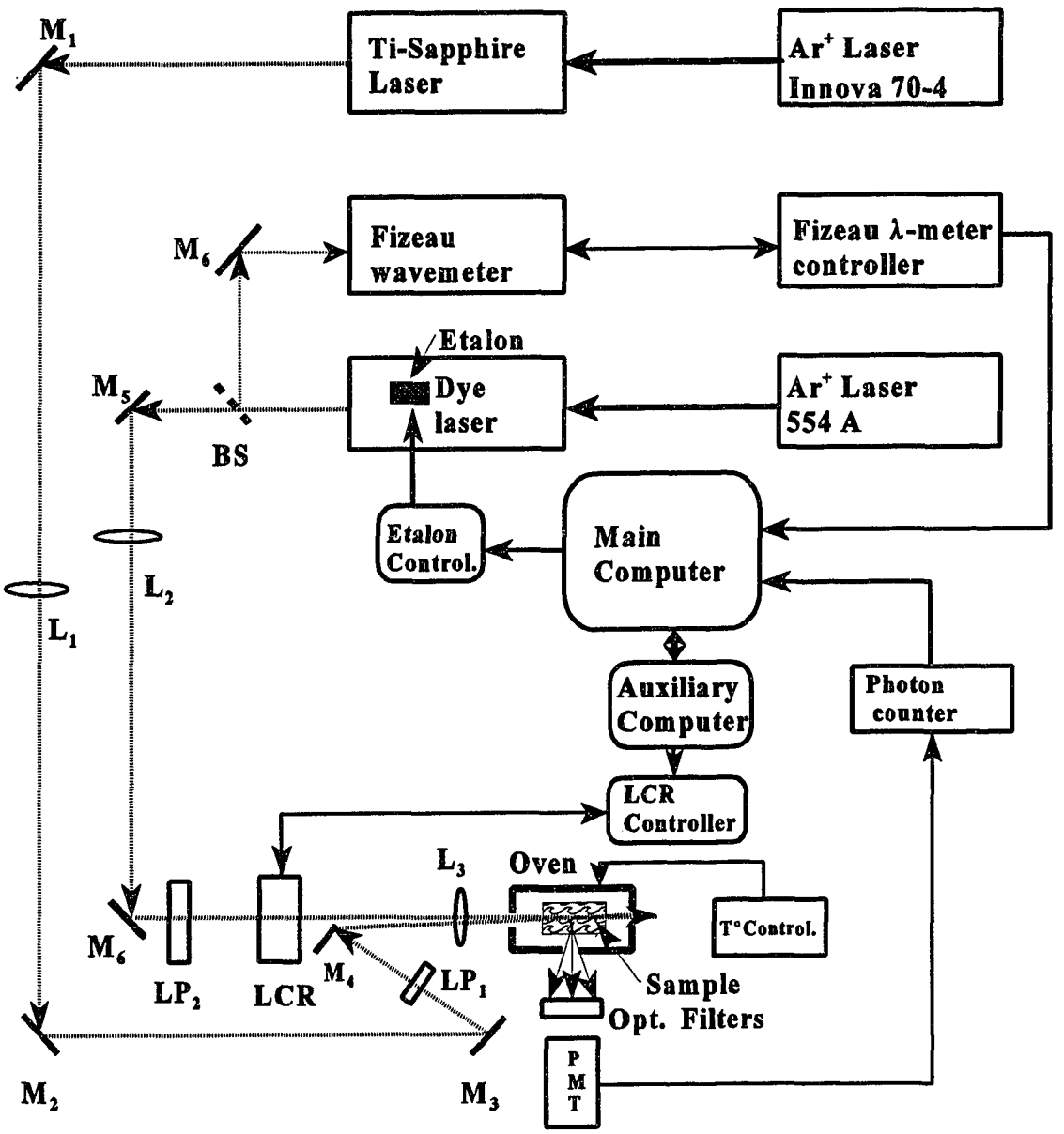


Figure 9. Schematic of the experimental device setup.

having an all-lines output on the order of 4.7 W, is used to pump a Titanium - Sapphire ring laser. The output of this laser (typically 400-500mW) is directed by a system of mirrors $M_1$, $M_2$, $M_3$ and $M_4$ into the sample cell, which is located in a temperature - controlled oven. The beam is focussed by lenses $L_1$ ($f \approx 150$ cm) and $L_3$ ($f=20$ cm). The polarization direction of this laser light is defined by a Glan-Thompson polarizer $LP_1$. Another $Ar^+$ ion laser, Holobeam Inc., Model 554A with all lines output power on the order of 3W is used to pump a standing-wave dye-laser. The output of this laser (500-700mW ) is directed into the sample cell by the mirrors $M_5$ and $M_6$ and it is focussed by the lenses $L_2$ ($f \approx 150$ cm) and $L_3$. The initial direction of polarization of this laser is defined by a Spindler & Hoyer polarizer $LP_2$ and can be rotated by 90° or preserved by the liquid crystal retarder LCR. A small portion of the intensity of this beam (~4%) is directed by the beam splitter (BS) and the mirror $M_7$ into a Fizeau wavemeter, Laser Technics Corporation, Model 100F (FWM), for precise wavelength measurement. The beams are focused and overlapped in the interaction region of the cell. The radius of the interaction region is approximately 35$\mu$m. The divergence of each beam, as well as the divergence between axes of the beams is estimated to be 25 mrad (~1.4°).

The two-photon absorption intensity is proportional to the intensity of the subsequent cascade fluorescence, which is detected by the photomultiplier tube (PMT), THORN - EMI, Model # 9235B, with a bialkali Rb-Cs photocathode. The appropriate spectral range of the fluorescence ($360 \pm 10$ nm) is filtered out by the Color Glass Filter UG1 (1mm) and an interference filter Oriel, Model # 53410 (Optical filters) installed in front of the photomultiplier tube. The individual photon signals from the photomultiplier

tube are directly counted by the photon counter, Stanford Research System, model SRS400, and the corresponding total numbers of counts per specified time intervals (one second) are stored in the main computer memory. During one experimental run this procedure is repeated two hundred times, as the frequency of the dye laser is scanned. This scanning is accomplished also by the main computer, which controls the frequency of the dye laser by changing, through a digital-to-analog converter, the voltage applied to the electromagnet, defining the angular position of the etalon (VIRGO optics, Inc, 1.00″ diameter×1mm thick.) and the birefringent filter in the dye laser. It also controls the direction of polarization of the beam 2 by issuing corresponding commands to the auxiliary computer, which contains a card installed for liquid crystal retarder control. The readout of the Fizeau wavemeter at each of 200 steps of the ~2 $cm^{-1}$ dye laser frequency scan, typical of each experimental run, is also stored in the main computer.

## III.3. Sample preparation

The objective of the sample preparation procedure is to place an atomic rubidium sample into a Pyrex cell (see Fig.10) and to have it sealed with minimal contamination of rubidium and minimal degradation of the optical quality of two flat cell windows. Rubidium metal, in natural isotopic abundance was supplied by Alfa Products Inc.

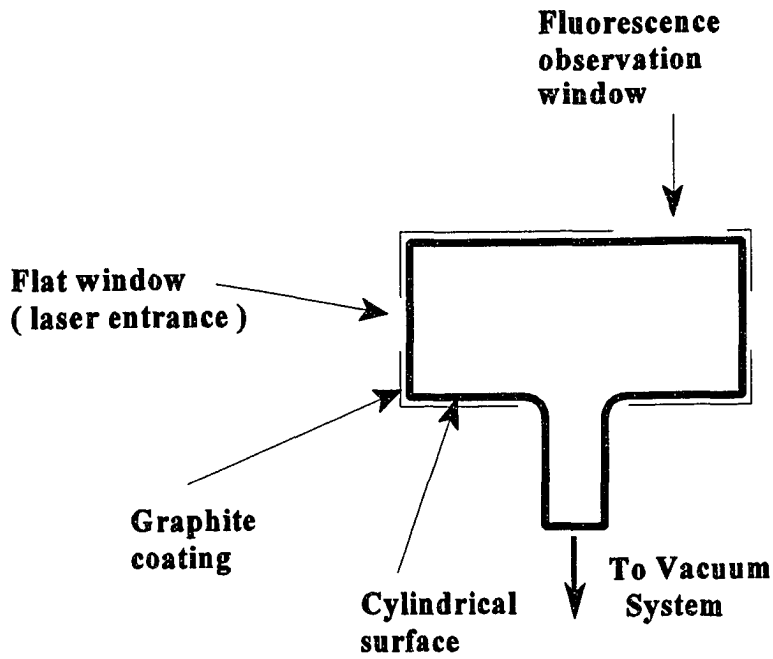


Figure 10. The sample container - Pyrex cell.

## III.3.1. Vacuum system

A capsule with rubidium metal, and the Pyrex cell were attached to the vacuum system by glass blowing. The schematic diagram of the vacuum system is shown in Fig.11. It consist of the fore vacuum pump, GCA/Precision Scientific, Model VAC TORR 150, the vacuum ion pump, Varian, Model 911-5034, and a system of pipes and valves. The vacuum measurement is accomplished by a Hastings Vacuum Gauge, Model SV-4, with Gauge Tube, Model DV-6M, two Capacitor Gauges, MKS Instruments, Model 221A, and, at the final stages of the vacuum preparation, by the control unit of the ion pump, Varian, model 921-0062. Ultimate vacuum achievable by this system is $10^{-8}$ Torr.

## III.3.2. Sample preparation technology

The initial check for leaks is performed using a High frequency spark generator (Tesla coil), Electro Technic Product company, Model BD10. If found, the leaks are removed. After this the system is evacuated to ~$10^{-6}$ Torr. If this level of vacuum can not be reached, microleaks causing this must be found and removed. Then a heating oven of heat resistant bricks is built around the rubidium capsule and cell, and a heating tape placed around all components of the vacuum system. The system is "baked" for ~ 48 hours at ~200°C. The temperature is controlled using a Cole - Palmer Instrument company Temperature Controller, Model 2186-10. When the system has cooled to room temperature, the vacuum level is typically ~$10^{-8}$ Torr. At this point the

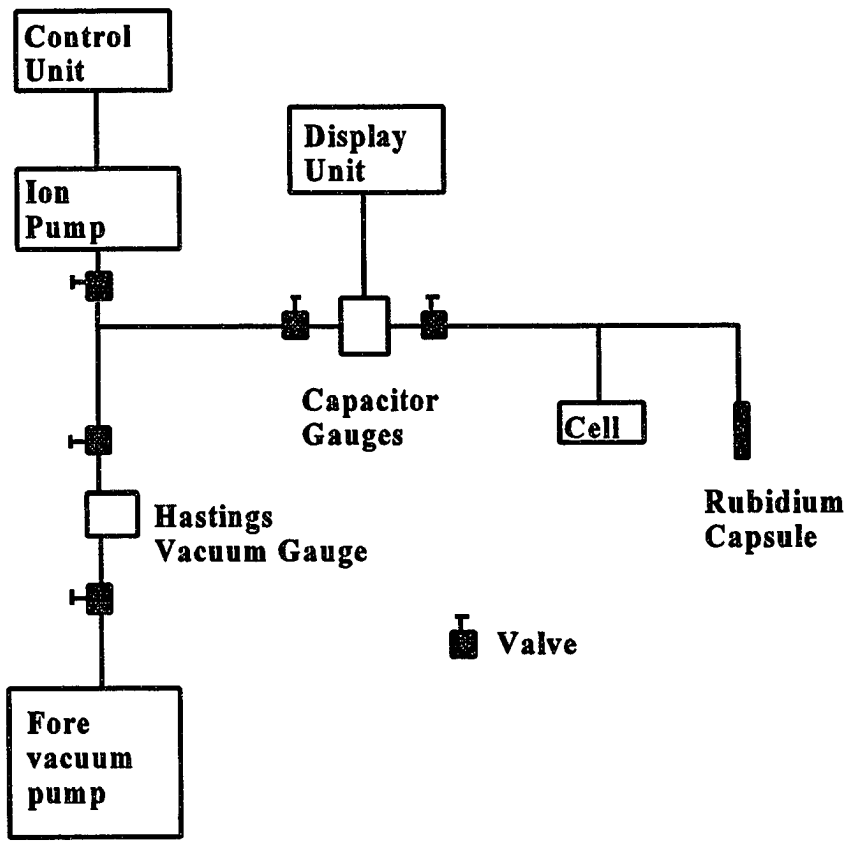


Figure 11. The vacuum system arrangement.

glass seal on the rubidium capsule is broken off using a "magnetic hammer" inside the vacuum pipe. The Argon buffer gas is then evacuated and the vacuum is restored to $\sim 10^{-8}$ Torr. Using a Bunsen burner, the rubidium is evaporated in small portions and forced to migrate along the pipes to the cell, until a considerable amount, on the order of $0.01 cm^3$, is accumulated in the cell. Then the cell is sealed off by glass blowing. During the whole procedure, special precautions are taken to prevent thermal stress on the cell windows. The absence of birefrigence in the cell windows was checked before and after this procedure by means of two crossed polarizers. No visible change was observed. The rigorous systematic check of the cell windows birefringence is described in section IV.

# III.4. Experimental device components

In this section we give a detailed description of the equipment, used in the experiment. Some of the early versions of equipment, replaced at the later stages of experiment, as well as some modification of equipment will be discussed.

## III.4.1. Lasers

The two photon transition $5s^2S_{1/2} \rightarrow 8s^2S_{1/2}$ in Rb can be achieved by use of two tunable light sources, one in the vicinity of 790 nm, and another in the vicinity of 610 nm (see Fig.12). Tunable lasers, as the most convenient light sources, were used in the

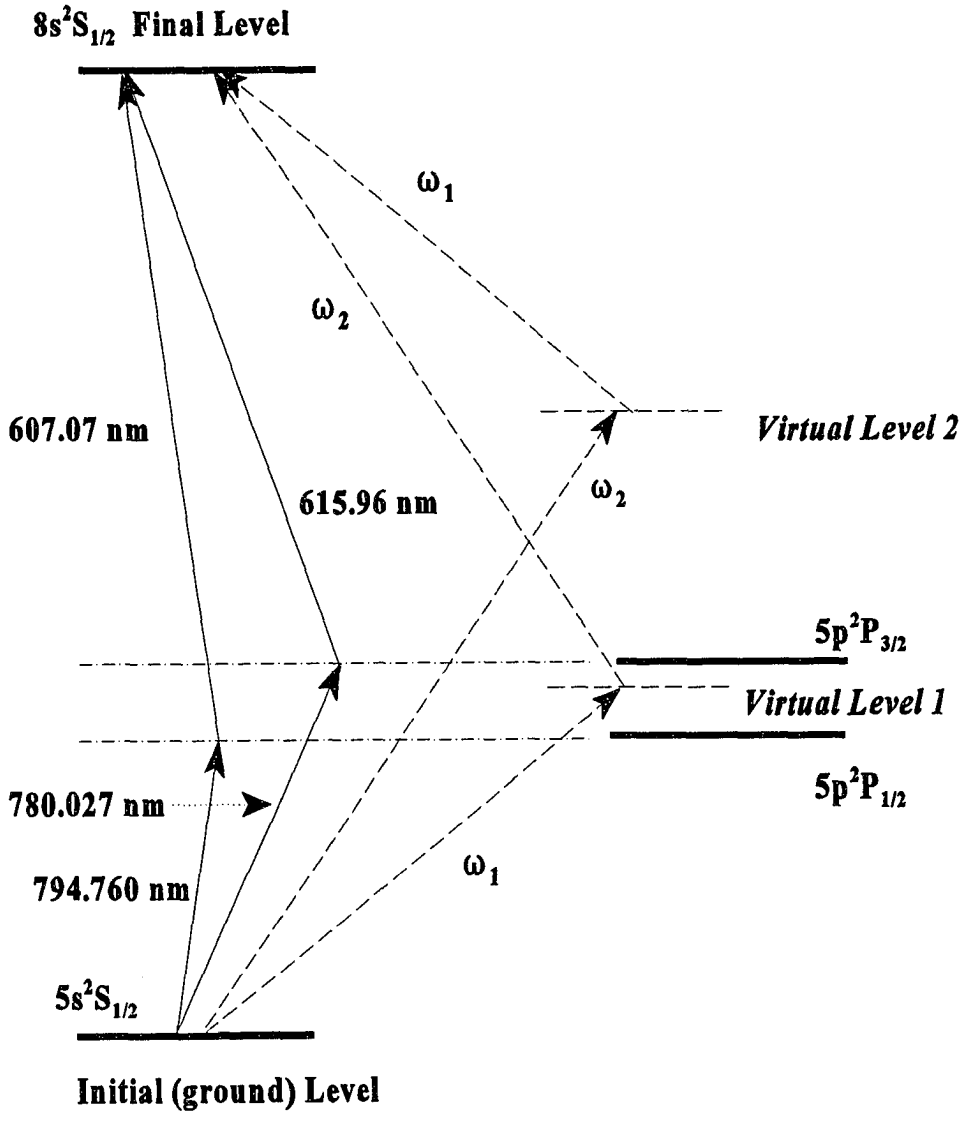


Figure 12. The wavelengths of the resonant $5s^2S_{1/2} \rightarrow 5p^2P_j \rightarrow 8s^2S_{1/2}$ transitions with j=1/2, 3/2.

experiment, namely a Titanium-Sapphire ring laser and a standing wave dye laser. The principles of laser operation are covered in many textbooks and articles, and will not be discussed here. As a short general reminder we mention that any laser contains two necessary components. First, it needs to have an active medium for amplification of the light and an optical resonator, which consists of a system of mirrors and stores the light energy in a specific (narrow) frequency region. The energy source, such as electric discharge,flash lamp or another laser, is necessary for laser light production. The tunable lasers additionally include tuning elements, such as birefringent plates or an etalon. In the following we will restrict our attention to the specific details of the lasers used in the experiment.

The coverage of the spectral range in the vicinity of 790 nm (infrared) represented a large obstacle at the initial stages of the experiment. In our first attempts, a Coherent Model 599 dye laser was used with LDS751 dye, the most appropriate for this spectral range (710 to 850 nm). This dye, however, is not very efficient and requires a relatively high lasing threshold pump power (broad band $Ar^+$ ion laser) [68]. The maximum power from the $Ar^+$ ion lasers available to us was close to 4.5W. With careful adjustment of the dye concentration, dye pump pressure, dye jet position and optical system of the dye laser the best results obtained were as follows: ~ 150 mW output power without birefringent filter, ~100 mW output power with birefringent filter at wavelength 765 nm, ~ 40 mW output power with birefringent filter at wavelength 780 nm. Although this power is low, it is sufficient to perform the experiment at a not-very-high level of precision. In fact, the first two-photon absorption signals were

obtained with this laser. But a much more significant problem, which made using this laser virtually impossible, was its frequency and intensity instability. The low pump power caused the operation of the dye laser to be near the threshold of the lasing, making it highly sensitive to small changes of environment temperature, dye solution pressure and small fluctuations of pump laser power. Therefore finally this laser was replaced by a Titanium-Sapphire ring laser, which normally operates with the available 4.5W pump laser power. The base configuration of the Coherent model 899-01 Titanium-Sapphire laser (shown in Fig.13) with three plate birefringent tuning element and a 1mm etalon, produces infrared light in the range 710 -840 nm with an output power 400 to 500 mW and a bandwidth close to 3 GHz. The bandwidth was measured by the Spectra-Physics spectrum analyzer, Model 476 (free spectral range 8 GHz). Data was taken using a digital-to-analog converter, Metrabyte Corporation, Model DAS-20, as an analog photodiode signal and stored in the computer. The data, along with the fitting curve, is shown in Fig.14. The full width at half maximum of the fitting curve is equal to 3.04 GHz. Fitting was performed using the graphic computer package Sigma-Plot 5.0. Without the 1mm etalon the estimated bandwidth is in the range from 8 GHz to 15 GHz. This estimation follows from the fact that no interference fringes were observed using the 8 GHz free-spectral-range analyzer, but they are visually observed using a 0.5 $cm^{-1}$ (15 GHz) free-spectral-range etalon. The former configuration of the Titanium-Sapphire laser was used at initial stages of the experiment

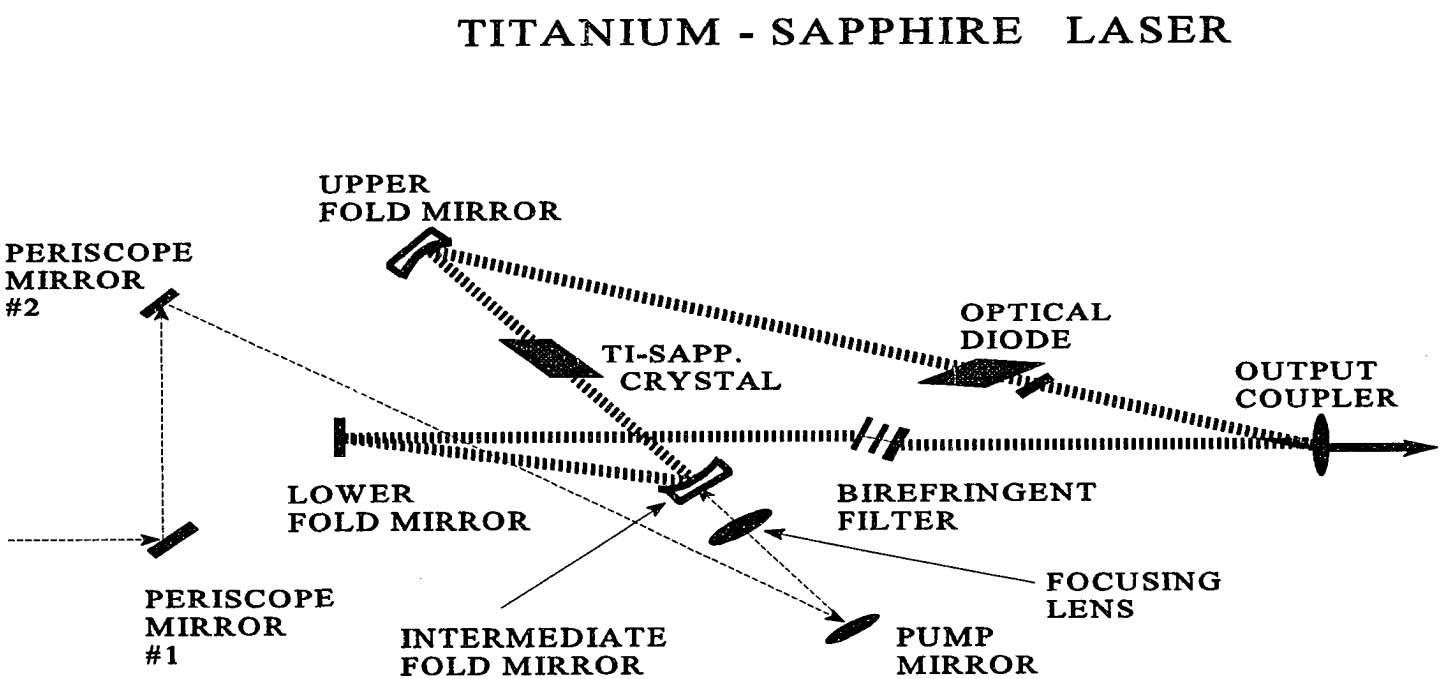


Figure 13. Schematic of Titanium - Sapphire laser.

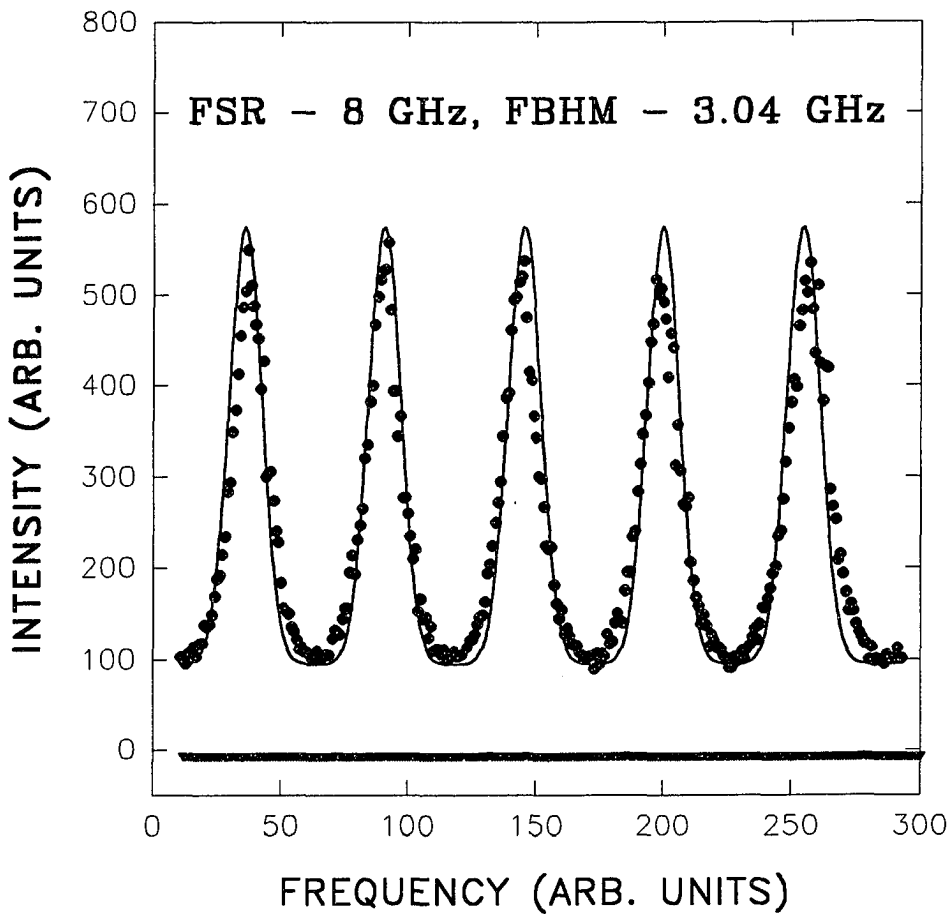


Figure 14. Titanium - Sapphire laser bandwidth determination. Free Spectral Range (FSR) of the spectrum analyzer is 8 GHz. Full Bandwidth at Half Maximum (FBHM) of the curve, fitted to the experimental points is 3.04 GHz.

and for some systematic tests, the latter configuration was used in all actual data taking procedures. Explanation for this choice is given in section IV.

The second spectral range, around 610 nm, is conveniently covered by dye lasers with the highly efficient dye Rhodamin 590. We used a Coherent, Model 599 dye laser in a standing wave configuration. A schematic of this laser is shown in Fig.15. Dye solution molar concentration is $2.1 \cdot 10^{-3}$ (solvent is ethylene-glycol and methanol). The concentration was adjusted to optimize the lasing in the required spectral region. A pump $Ar^+$ ion laser (Holobeam inc.,Model 554A) power on the order of 3 W was used, sufficient to produce dye laser output beam power from 500 to 700 mW. The bandwidth of about 5.58 GHz was obtained with a three-plate birefringent tuning element and a 1mm etalon. The change of angular position of the etalon, with appropriate adjustment of birefringent filter position, provides the change of the central frequency in a range of $\sim 2cm^{-1}$ in each experiment (the purpose of this so-called scanning procedure will be explained later). The bandwidth was measured by the spectral analyzer, described earlier. Data from the bandwidth measurement is presented in Fig.16. The fitting procedure was similar to the one used for the Titanium-Sapphire laser.

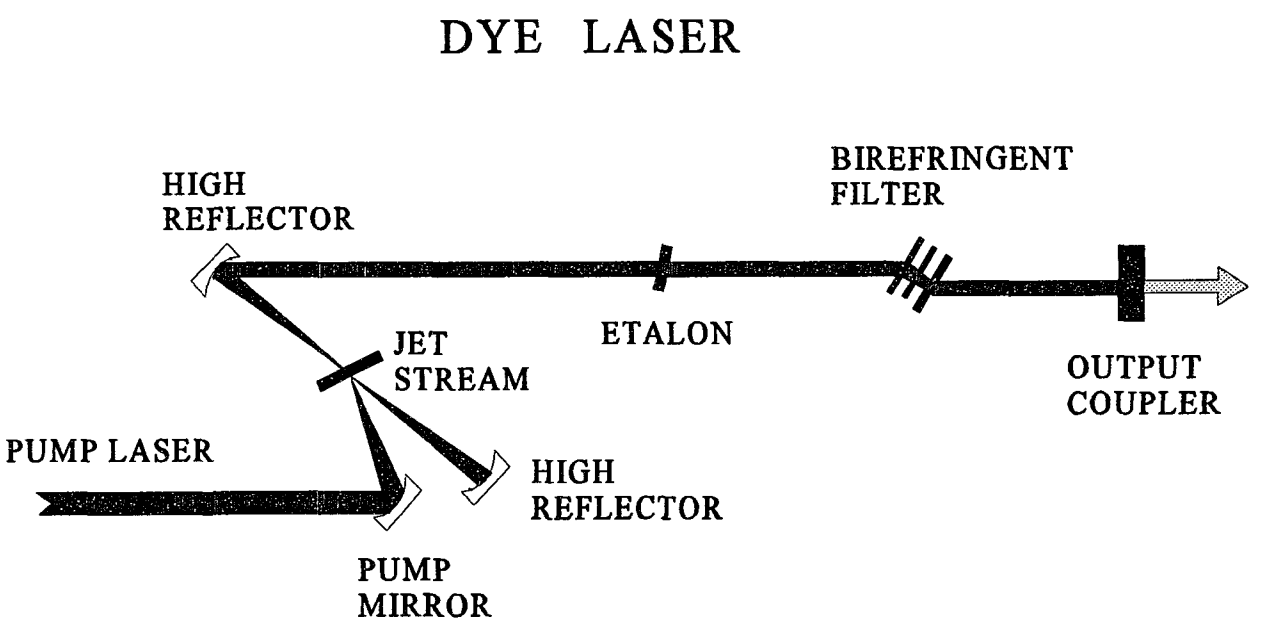


Figure 15. Schematic of Dye laser.

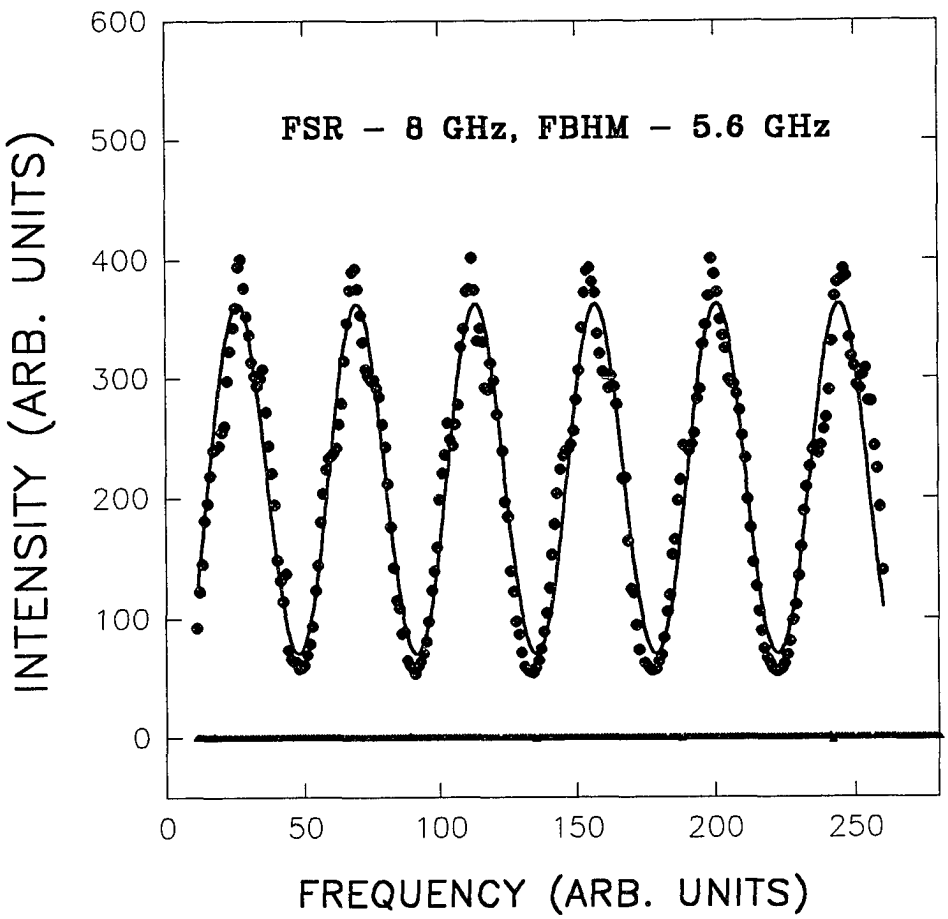


Figure 16. Dye laser bandwidth determination. Free Spectral Range (FSR) of the spectrum analyzer is 8 GHz. Full Bandwidth at Half Maximum (FBHM) of the curve, fitted to the experimental points is 5.60 GHz.

## III.4.2. Polarization of the light

Both light beams produced by lasers are nearly linearly polarized in the vertical plane. The polarization of the light is altered to some extent as it passes through several devices to the sample cell (see Fig.9). In order to define the linear polarization of the light with high precision, very high quality polarizers were used. Polarization of the light produced by the dye laser (this light beam will be referred to in the following as beam 2) was defined by a Spindler & Hoyer, Model 10K, polarizer, with a quoted extinction ratio 1:10000 ($LP_2$ in Fig.9). This polarization direction was kept unchanged during all experiments and at each run was used as a reference for setting the direction of polarization of the light produced by the Titanium-Sapphire laser (hereinafter referred to as beam 1), and for alignment of an analyzing device, as described in the following section. The precise polarization direction of beam 1 was defined by a Newport Research Corporation Glan-Thompson polarizer, Model 10GTO 4ar.14, with an extinction ratio 1:10000 ($LP_1$ in Fig.9). Angular position of this polarizer was controlled by means of a high quality positioning device with precision better than 1.8 mrad (0.1°). Alignment of this polarizer with the direction of propagation of beam 1 for nearly normal incidence was achieved by means of retroreflection at the start of each experiment. This was one of the necessary conditions for reliable $\pm 45°$ tests (see next section). The satisfactory $\pm 45°$ tests allowed proper setting of the direction of

polarization of beam 1 for an entire set of experimental runs at a given detuning (3-5 runs). For analyzing the quality of the beam polarizations, an Oriel Corporation Wollaston Polarizer, Model 25697 with extinction ratio 1:10000 was used (not shown in Fig.9). This polarizer was aligned for nearly normal incidence of the beams by means of retroreflection. Its proper angular position was established using beam 2 as a reference by minimizing the power of one of the Wollaston Polarizer output beams. In the experiment, the direction of polarization of the beam 1 does not change, but the direction of polarization of the beam 2 is changed once per second from vertical to horizontal and back. This rotation of polarization direction is accomplished by a Meadowlark Optics liquid crystal retarder, Model LVR-0.7-700 (LCR in Fig.9). The proper installation of this device in the path of beam 2, its physical positioning and adjustment of its electronic settings (via computer interface, Meadowlark Optics, Model D1040) is one of the most critical and technically difficult parts of each experimental procedure. The difficulty is due to the fact, that the quoted accuracy of the retardance of 0.3% was actually considerably improved in every experimental run by fine adjustments to yield a typical contrast ratio for both directions of polarization on the order of 1:4000. This contrast ratio was measured by the Newport Research power meter, Model 815, as a ratio of the powers of the output beams of the Wollaston polarizer. Monitoring of the weak output beam of the Wollaston polarizer, at its installation as well as at the installation of the Glan-Thompson polarizer is conveniently

accomplished by use of the power meter head with an oscilloscope. The fluctuations of the digital readout of the power meter control unit at powers close to the lower limit of sensitivity of this device were thus avoided.

## III.4.2.1. Optical polarizers

In this section we give a short description of the principles of operation of the optical polarizers used in the experiment. The Spindler & Hoya polarizer, model 10K, belongs to the family of polarizers in which the polarization selective transmittance is achieved by means of oriented polymer chains with imbedded crystals. The unpolarized light loses its component polarized parallel to the direction of the polymer chains because of high absorption. As a result, the transmitted light is linearly polarized, as shown in Fig.17. The quality of the device is quantitatively characterized by an extinction ratio: the ratio of the minimum of the transmission coefficient, when incident light is linearly polarized in direction parallel to the direction of the polymer chains, to the maximum of the transmission coefficient, when polarization of the incident light is perpendicular to the direction of the polymer chains. In other words, it is a ratio of the mutually perpendicular linearly polarized weakest and strongest components of the transmitted light, when the incident light is unpolarized, or when it is circularly polarized. The

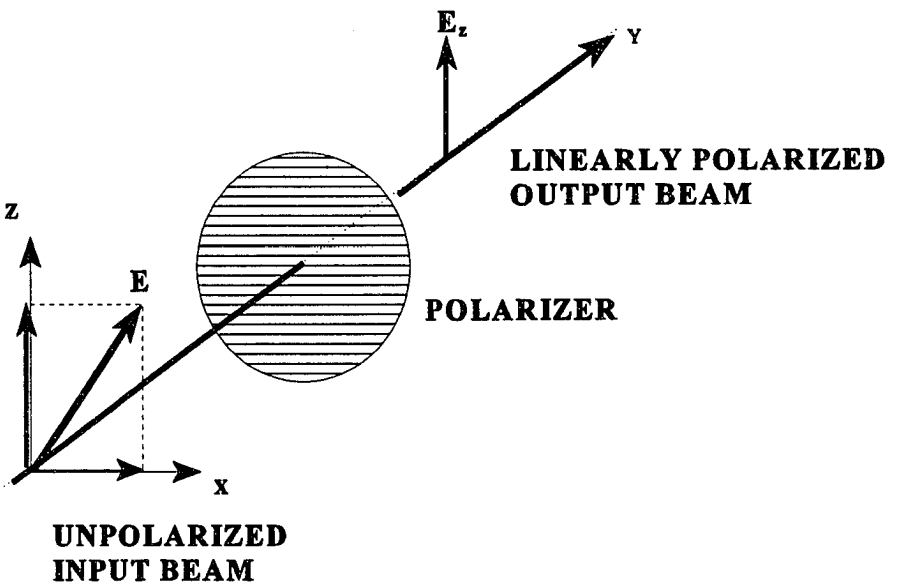


Figure 17. Principle of the Spindler & Hoyer polarizer.

quoted extinction ratio in our case was 1:10000. The operation of the two other polarizers, used in the experiment, the Wollaston polarizer and the Glan-Thompson polarizer, is based on the property of uniaxial crystals to exhibit a different index of refraction depending on the polarization of the light. Accordingly, a beam of light with proper direction of propagation and with an arbitrary polarization will be physically split in such a crystal into two beams, one with polarization direction perpendicular to the crystal axis (called an ordinary beam), and the other with direction of polarization perpendicular to the first (called extraordinary). Both polarizers are designed as a combination of two prisms (see Fig.18 and Fig.19). In the Glan-Thompson polarizer, which is a modification of the Nicol prism, the ordinary beam experiences total internal reflection at the interface of the prisms and is subsequently absorbed. The output extraordinary beam is linearly polarized. The Wollaston polarizer is designed to provide large angular separation of the ordinary and the extraordinary beams, which as the two output beams, are linearly polarized in mutually perpendicular planes. The quoted extinction ratio for both devices is 1:10000.

As already described, for the 90° rotation of the direction of polarization of beam 2, the liquid crystal retarder was used. In the liquid crystal, a medium with an orderly arrangement of long, rod shaped molecules in a liquid phase, the mutual orientation of the molecules is defined by the properties of the specially prepared optical windows of the container and by the applied control voltages. These, in turn, define the polarization

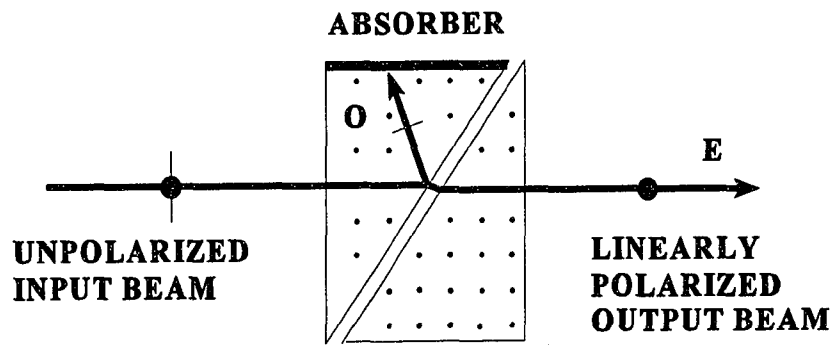


**O - *ORDINARY BEAM***

**E - *EXTRAORDINARY BEAM***

Figure 18. Principle of the Glan - Thompson polarizer.

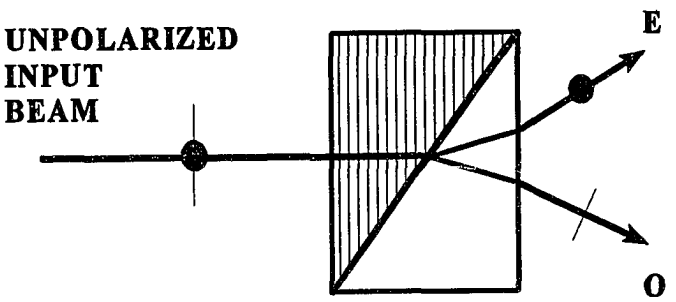


**O** - ***ORDINARY BEAM***

**E** - ***EXTRAORDINARY BEAM***

Figure 19. Principle of the Wollaston polarizer.

direction of the transmitted light. By proper positioning of the device and fine adjustments of the control voltages, we were able to achieve a typical contrast ratio of 1:4000 for both directions of polarization of the output beam.

## III.4.3. Frequency control of the dye laser

During each experimental run the frequency of the Titanium-Sapphire laser was fixed, and the frequency of the dye laser was changed in two hundred small steps over an interval of ~2.0 $cm^{-1}$ . The purpose of this "scanning" procedure was two-fold. First of all, it allowed reliable definition of the background level as the number of photocounts in the first and the last approximate quarters of the scan (see Fig.20). Secondly, it effectively averaged the signal over all hyperfine structure components of the levels involved in the two-photon transition. By doing this a null effect of hyperfine structure was assured (see section II.6).

It seems natural to have scanned the Titanium-Sapphire laser frequency, because the dye-laser light polarization is being rotated and the effect of the liquid crystal retarder, used for rotation,generally speaking, is frequency dependent. However, scanning the Titanium-Sapphire laser was found to be impossible. Our method of scanning requires

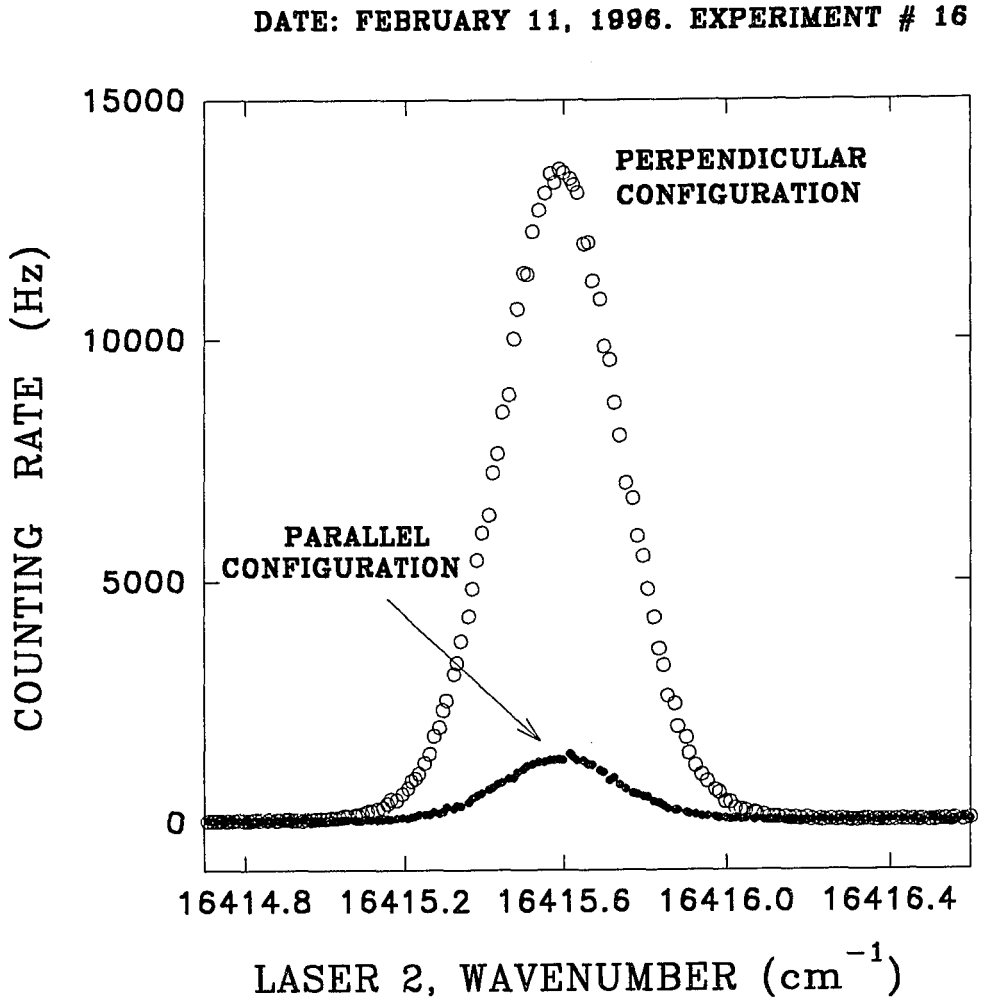


Figure 20. Result of a typical experimental measurement. Counting rate as a function of the relative polarization of lasers and wavenumber of the scanned laser (laser 2).

an etalon in the laser cavity, which also narrows the laser bandwidth. Installation of the etalon in the Titanium-Sapphire laser caused so much narrowing, that the partial resolution of the hyperfine structure had a pronounced effect on the results of the polarization degree measurements. On the other hand, we found that scanning had no effect on the performance of the liquid crystal retarder at our experimental precision. Therefore the etalon was removed from the Titanium-Sapphire laser and the frequency of the dye laser was scanned.

The frequency was scanned by changing the angular position of the etalon in the laser cavity. The etalon is mounted on the arm of a galvanometer and rotated when an applied voltage changes. This change is controlled by the main computer as follows. The output analog voltage of the digital to analog converter, Metrabyte Corp., Model DAS-20, is set by the main computer, combined with the voltage from a precision source, Sorensen Power Supplies, Model QHS 40-.5 and applied to the galvanometer, as shown in Fig.21. During the scan the wavelength is measured by a Fizeau wave-meter. This high precision device under certain conditions showed a repeatable malfunction: the readout wavenumber increased by 5.0 $cm^{-1}$ without actual change of the laser frequency. This caused an irrecoverable interruption of the experimental run routine. We speculate that this was caused by partial failure of some electronic component of the devise. The simple and reliable way around this problem was achieved by a small rotation of the birefringent filter by an electromagnet when

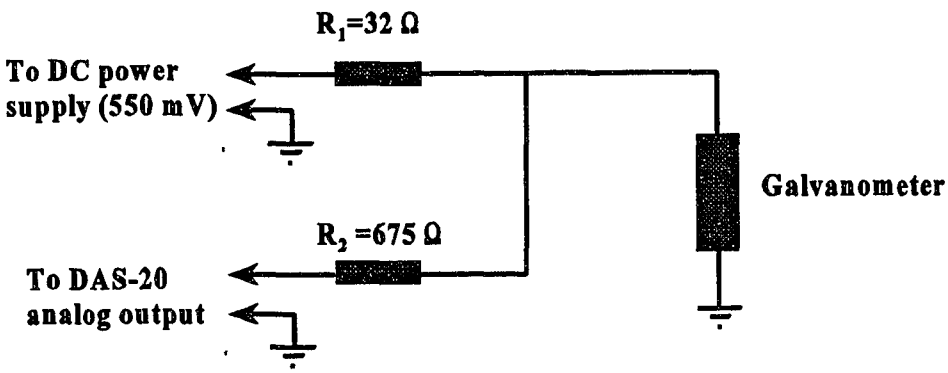


Figure 21. Circuit for controlling the position of the etalon in the laser cavity. The etalon is mounted on the galvanometer arm.

approximately 7/8 of a run was completed. This small rotation brought the central frequency of the laser, defined by the position of the birefringent filter, closer to the actual output frequency, defined by the etalon, without changing the latter. This caused the mentioned malfunction to disappear. The schematic diagram of the circuit controlling the electromagnet is shown in Fig.22. The command from the main computer issued to the digital to analog converter, activates the electromagnet, which through the lever, adjust the position of the birefringent filter.

## III.4.4. The Fizeau wavemeter

The Fizeau wavemeter is a device used for precise measurement of the wavelength of the dye laser light. The quoted accuracy is one part in $10^6$ . The wavemeter consists of the Optical Component Package, Controller, and the Display Unit. A schematic of the Optical Component Package is shown in Fig.23. The laser beam whose wavelength is to be measured, is shone into the wavemeter by the external Far Mirror and Near Mirror. The laser beam enters the wavemeter through the Input Aperture (IA). The intensity of the beam is adjusted by a Variable Attenuator (VA). Then the beam is directed by the two Turning Mirrors (TM1 and TM2) into a Microscope Objective (MO), and focused into a Pinhole (PH). This spatially filters the beam. The expanding beam is collimated by the Off-Axis Parabolic Mirror (OAPM) and directed onto a

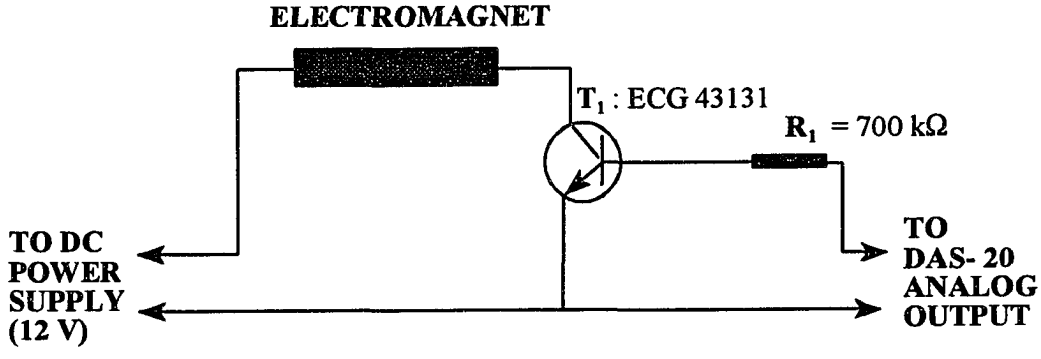


Figure 22. Circuit for controlling the electromagnet, rotating the birefringent filter of the scanned laser.

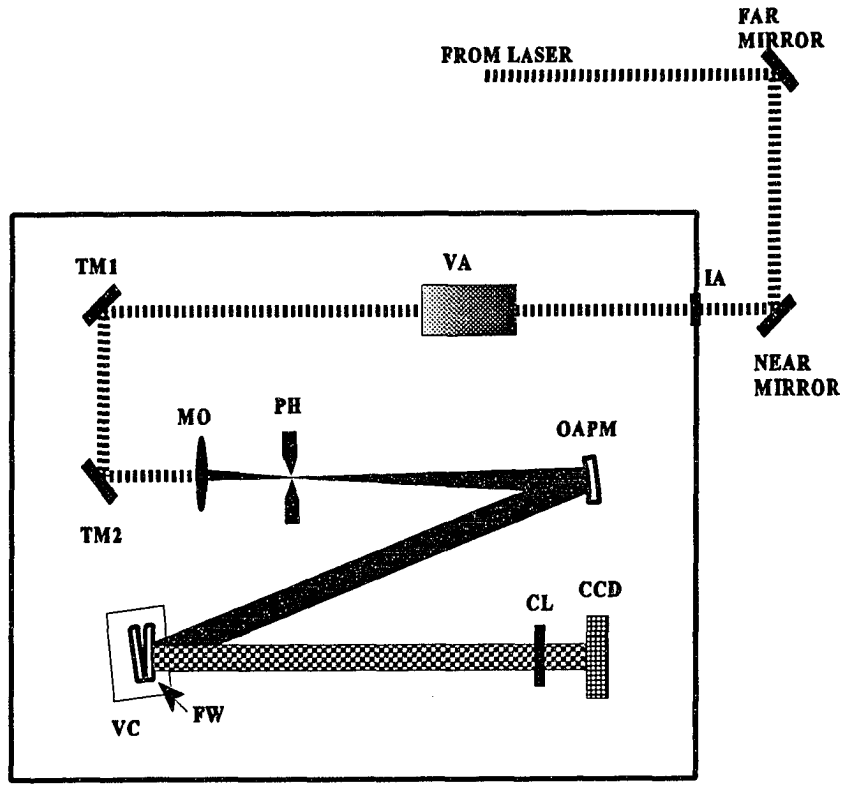


Figure 23. Schematic of the Fizeau wavemeter.

Fizeau wedge. The Fizeau wedge consists of two optical plates and a small spacer and is mounted in the Vacuum Can (VC). A beam reflected from its inner surfaces creates an interference pattern, in the form of parallel straight lines, which is focused by a Cylindrical Lens (CL) onto a linear 1024 element CCD Array. The interference pattern recorded in the CCD is used to determine the wavelength by the Controller unit and sent through the RS-232 digital interface to the Main Computer.

## III.5. Signal detection

The intensity of the cascade fluorescence $7p^2P_j \rightarrow 5s^2S_{1/2}$ at ~359 nm is used as a measure of the two-photon $5s^2S_{1/2} \rightarrow 8s^2S_{1/2}$ absorption rate (see Fig.24). For detection of this fluorescence a THORN-EMI Electron Tubes, Model 9235B, photomultiplier tube with a bialkali photocathode (Rb,Cs) was used. In front of the photomultiplier tube a color glass filter UG1 (1mm) and an interference filter, Oriel, Model #53410 were installed to filter out the spectral region of interest. The number of the photoevents was counted by the photon counter SR400 and sent into the main computer throught the RS-232 digital interface.

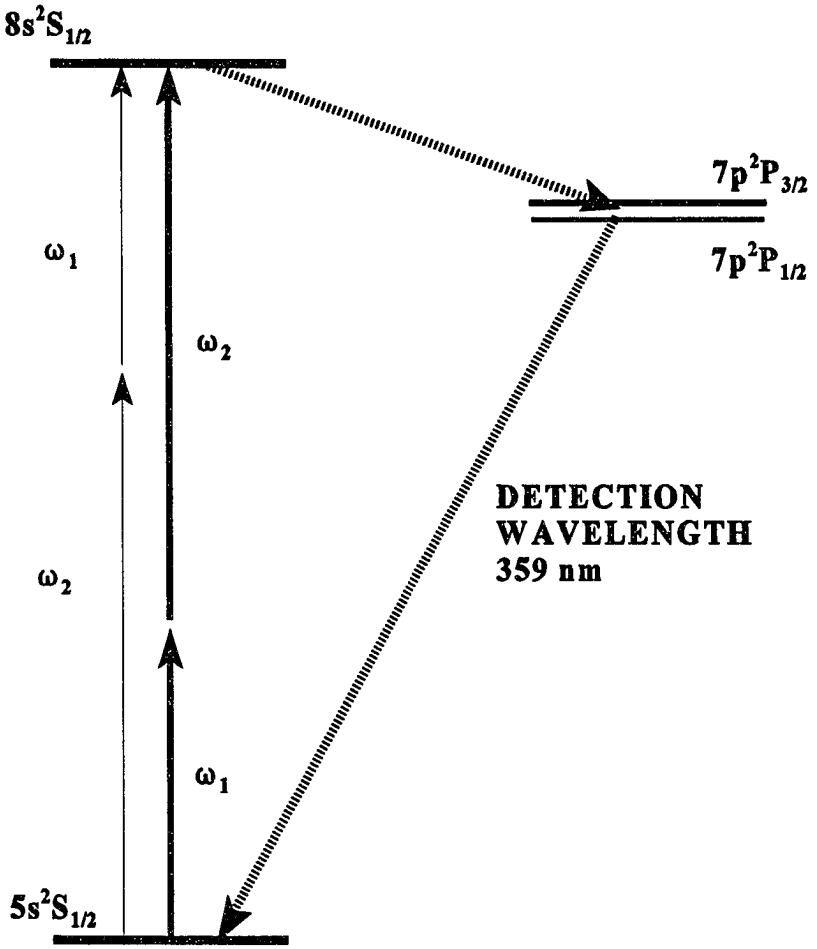


Figure 24. The wavelength of the signal observation.

# III.6. Device preparation

Each daily experimental procedure included the following preparation steps:

#1 Turne the lasers and the electronic equipment on and wait for temperature stabiliza tion.

#2 Tune the lasers for maximum power and $TEM_{00}$ mode.

#3 Align the probe beam pickup with the Fizeau wavemeter.

#4 Tune the probe laser to the target wavelength.

#5 Adjust the direction and size of the laser beams to achieve nearly colinear (~25 mrad) beams, low divergence (~25 mrad) and intersection in a narrow (~35 $\mu$m radius) interaction region.

#6 Install the Glan-Thompson polarizer in the pump beam and the Spindler&Hoyer polarizer in the probe beam at normal incidence.

#7 Install and align the analyzer (Wollaston prism) with polarization of the probe beam ( minimum light intensity monitored using the power meter head and the oscilloscope ).

#8 Angularly align the Glan-Thompson polarizer with the analyzer ( minimum light intensity monitored using the power meter head and oscilloscope ; this yields the

initial direction of pump polarization corresponding to parallel pump and probe polarization ).

#9 Install the Liquid Crystal Retarder (LCR) in the probe beam and coarsely align the optical axis with the probe beam initial polarization at $\lambda/2$ retardance by manually rotating the LCR and visually observing the minimum intensity of the correspond ing analyzer output.

#10 Performe fine angular adjustment of the LCR ( minimum light intensity monitored using power meter).

#11 Electronicaly adjust the LCR $\lambda/2$ retardance at target wavelength (Fizeau readout).

#12 Same for zero retardance.

#13 Start the computer program controlling the LCR with settings for retardancies obtained in #11 and #12.

#14 Remove the analyzer, install the cell with the Rb sample at the intersection of the beams and set the temperature of the sample.

#15 Observe the two-photon signal by the photomultiplier tube and maximize it by adjusting the photomultiplier tube position, cell axial position and micrometer controls of the probe beam.

# 16 Perform the polarization measurements at angular positions of the Glan-Thompson polarizer $\pm 45°$ from the original position ( pump polarization direction $\pm 45°$

from direction of the original polarization of probe).

Note that a result of step #16 equal to $\pm.2$ (.2) % is considered as satisfactory. In this case the device is ready for routine measurement of the polarization degree at the set detuning. Otherwise steps #6 to #16 are repeated until step #16 yield a satisfactory result.

## III.7. Measurement process

After the devices have been prepared, the process of data collection is controlled by a computer program, coded in Quick Basic, running on the main computer. At the early stages of the experiment, the sequence of steps in the data collection was following. First, the initial wavelength was set by proper positioning of the etalon. Then the polarization of the probe was set in parallel configuration. The fluorescence photons were counted during one second. Then polarization of the probe was set in perpendicular configuration and fluorescence photons were counted during one second. This was repeated 200 times at all increments of the frequency of the probe laser. It was realized in course of the experiment, that in such mode of the data collection, the slow drift of the Titanium-Sapphire laser frequency can cause a considerable effect because of the

possible distortion of the signal curve shape. To reduce the effect we buffered the cooling water for the Titanium-Sapphire laser medium. Also the protocol of the data collection procedure was changed. Namely, the order of parallel and perpendicular configurations of the polarizations of lasers was inversed at each step of the scan. This reduced the effect of the slow drift of the Titanium-Sapphire laser frequency, and reduced the number of polarization switches per run by a factor of 2. Thus the time of one experimental run was shortened from ~20 min to ~15 min. The result of a typical experimental run is shown in Fig.20.

# IV. Systematic tests

The systematic tests are specific experimental procedures, designed to reveal systematic errors which must subsequently be removed or properly accounted for. The systematic errors inevitably occur as a result of repeatable improper functioning of experimental devices or repeatable peculiar experimental conditions, which were not understood adequately. Such effects can cause repeatable shifts of the results of experiments, and, if not identified, result in erroneous experimental outcomes. In order

to test the experimental devices against systematic errors, their functions must be compared with functions of similar (external) devices. Differences would then indicate a problem. To find these errors, the routine experimental conditions must be altered to the highest possible degree. If such alterations cause changes in the experimental results, the mechanism of these changes must be understood and measures taken to either avoid them in the routine experiment or to properly account for them. This sort of experimental procedures is most effective if a preliminary idea of a possible systematic effect is present. But they must be performed even if no systematic effects seem to be likely *a priori*: systematic tests can sometimes prove the preliminary guess to be wrong.

This section discribes the systematic tests we have performed. It starts with a detailed consideration of two examples, typical and instructive, and then continues with a brief description of the remainder. The first example is concernes the performance of the photomultiplier tube and photon counter. Our initial settings of the discriminator level and PMT voltage to optimize the signal to noise ratio were 110mV and 950V respectively. In the course of the polarization measurements it was observed that the absolute value of $P_L$ increased if the rate of photon counting was increased. After a helpful discussion of this matter with the technical personnel of the manufacturer of the photomultiplier tube, THORN-EMI Electron Tubes, it was realized that one possible cause of the problem is registration by the PMT of multiphoton events. We performed

a set of careful tests and found that this was a most likely cause. The problem was corrected by lowering the discriminator voltage to 55mV, PMT voltage to 820V, and restricting the maximum counting rate to about 15000 $s^{-1}$. The explanation is as follows. If the counting system registers only single - photon events, then

$$\begin{aligned} n_{\parallel} &= \alpha' I_{\parallel} \\ n_{\perp} &= \alpha' I_{\perp} \end{aligned} \tag{48}$$

where $n_{\parallel}$ ($n_{\perp}$) is the number of counted photons per second in the parallel (perpendicular) configuration, $I_{\parallel}$ ($I_{\perp}$) is the corresponding intensity of the fluorescence from the interaction region of the sample, and $\alpha'$ is some proportionality constant. In this case the measured polarization degree

$$P'_L = \frac{n_{\parallel} - n_{\perp}}{n_{\parallel} + n_{\perp}} = \frac{I_{\parallel} - I_{\perp}}{I_{\parallel} + I_{\perp}} \tag{49}$$

has the correct numerical value and will not change if the intensity changes, for example, by changing the sample density or laser(s) power. If the counting system registers only two-photon events, then there will be no change in the measured value of $P_L$ with changing $I_{\parallel}$ and $I_{\perp}$ although in this case the numerical value of $P_L$ will be wrong. In this case one has :

$$n_{\parallel 2} = \beta' I_{\parallel}^2$$
$$n_{\perp 2} = \beta' I_{\perp}^2 \qquad (50)$$

where $\beta'$ is another proportionality constant and

$$P'_L = \frac{n_{\parallel 2} - n_{\perp 2}}{n_{\parallel 2} + n_{\perp 2}} = \frac{I_{\parallel}^2 - I_{\perp}^2}{I_{\parallel}^2 + I_{\perp}^2} \qquad (51)$$

The quadratic dependence in eq.(50) reflects the fact that the probability of two photons arriving at the photomultiplier tube cathode at the same time is taken to be a product of the probabilities of two independent single-photon events.

In the case, when the counting system register both kind of events, one ($n_{\parallel 1}$,$n_{\perp 1}$) and two photon ($n_{\parallel 2}$,$n_{\perp 2}$), the measured polarization degree is

$$P'_L = \frac{(I_{\parallel} - I_{\perp}) + \alpha (I_{\parallel}^2 - I_{\perp}^2)}{(I_{\parallel} + I_{\perp}) + \alpha (I_{\parallel}^2 + I_{\perp}^2)} \qquad (52)$$

where

$$\alpha \equiv \frac{\beta'}{\alpha'} \qquad (53)$$

The numerical value of $P'_L$ will be close to the correct one if

$$n_{\parallel 1} \gg n_{\parallel 2}$$
$$n_{\perp 1} \gg n_{\perp 2} \qquad (54)$$

In this case to a good approximation

$$P'_L = P_L + \alpha I_{\parallel} P_L ( 1 - P_L ) \qquad (55)$$

At a discriminator level of 55mV the measured $P_L$ at fixed detuning and varying counting rate ( from 21,000 to 330,000 $s^{-1}$) yielded a value of $\alpha$ equal to $1.32 \times 10^{-8}$ sec/counts. Thus the nonlinearity of the counting system, at the counting rate close to 15000 $sec^{-1}$ will produce a shift in the measured $P_L$ close to $2 \times 10^{-4}$ , which is approximately 10 times smaller, than the typical statistical uncertainty of $P_L$, and can therefore be neglected. At a discriminator level of 110mV the effect of the two photon events became severely enhanced. As a result of this systematic test, the a new investigation of optimal parameters (photomultiplier tube voltage and discriminator level setting) for the best signal/noise ratio was carried out. With new parameters, tube voltage -820V and discriminator setting 55mV and maximum counting rate close to 15000 $s^{-1}$ the problem was eliminated. The readout of the photon counter SR400 was checked against the readout of the Synthesizer / Level Generator, Hewlett Packard, Model 3336C ; these were identical.

Another example of a systematic test is the investigation of the effect of the width of

the two-photon resonance signal on the measured polarization degree. At the initial stages of the experiment the two laser beams were counterpropagating and etalons were present in both lasers. These conditions are technically most convenient: alignment of the laser beams is easier when they are counterpropagating,and the frequency of the laser light is reliably controlled by the angular position of the etalon, as described earlier. Unfortunately these conditions also lead to the most narrow two-photon signals. First of all, the Doppler broadening is almost absent for the **counterpropagating** beams case [58], while in the case of **copropagating** beams at the typical experimental temperatures (80°C) the Doppler broadening is on the order of 4 GHz. Secondly, as already discussed, the bandwidth of the Titanium-Sapphire laser with the etalon is approximately 3 GHz, but without it is between 8 GHz and 15 GHz. The two photon signal shape, in the most narrow case, indicates the partial resolution of the ground state hyperfine structure. The clear indication of this can be seen in a following argument. In the configuration under discussion (narrow Titanium-Sapphire laser) the lasers widths are 0.101 $cm^{-1}$ and 0.186 $cm^{-1}$. The corresponding convoluted bandwidth is equal to .21$cm^{-1}$ . Ignoring the excited state hyperfine splitting, one can represent the shape of the signal by the sum of four Lorentzian profile functions of halfwidth 0.21$cm^{-1}$, centered at -0.0853$cm^{-1}$, -0.042$cm^{-1}$ +0.059 $cm^{-1}$ and +0.142$cm^{-1}$ (isotope shift is included) with amplitudes equal to the degeneracy of the corresponding ground state hyperfine component weighted by the natural abundance of the isotope, i.e. 1.4;

5.04; 3.60; 0.84 respectively:

$$\begin{aligned}
\rho_1 &= 1.40e^{-\frac{1}{2}\left(\frac{k+0.0853}{0.21}\right)^2} && (F=2;^{87}Rb)\\
\rho_2 &= 5.04e^{-\frac{1}{2}\left(\frac{k+0.0420}{0.21}\right)^2} && (F=3;^{85}Rb)\\
\rho_3 &= 3.60e^{-\frac{1}{2}\left(\frac{k-0.0590}{0.21}\right)^2} && (F=2;^{85}Rb)\\
\rho_4 &= 0.84e^{-\frac{1}{2}\left(\frac{k-0.1420}{0.21}\right)^2} && (F=1;^{87}Rb)
\end{aligned} \qquad (56)$$

The resulting function is shown in Fig.25 and its shape is similar to the shape of the real signal, with two pronounced peaks, Fig.26.

The partial resolution of the hyperfine components can result in so-called "optical pumping" [66a,69]. In the present experiment, the typical linear dimension of the interaction region is on the order of 100$\mu$m. The atom with the typical thermal velocity of 300m/s will spend approximately $3\times10^{-7}$ s in this region, which can be several times longer for the atoms, traveling in axial direction (y-axis on Fig.4). This is the same order as the decay time for an atom excited to the $8s^2S_{1/2}$ level [27]. Therefore it is likely, that a significant (in a high precision experiment point of view) fraction of the atoms will participate in two-photon absorption more than once before leaving the interaction region. For such atoms the effect of optical pumping among the ground state hyperfine levels will take place with subsequent change of the absolute value of

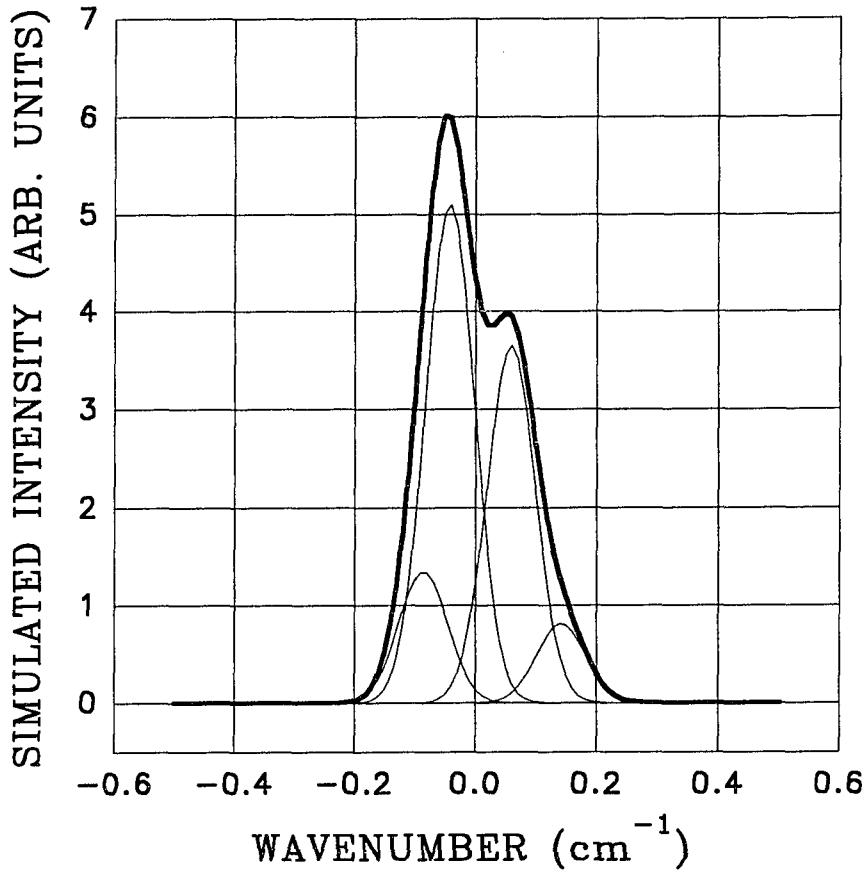


Figure 25. Sum of the four intensities due to the ground state hyperfine components of rubidium.

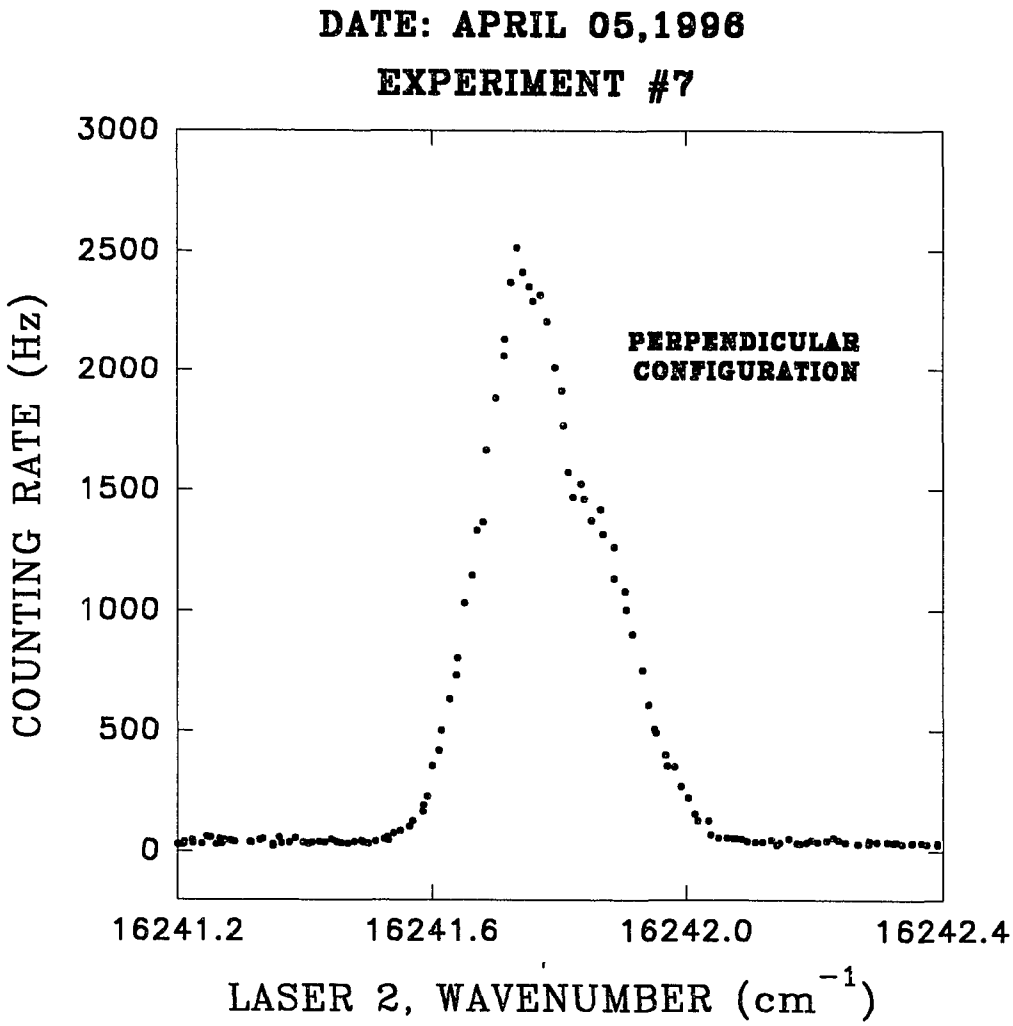


Figure 26. Experimental data. Narrow Titanium - Sapphire laser.

the measured polarization degree, an effect we actually observed. An appropriate rearrangement of the experiment excluded this effect completely. We achieved the broadest possible two-photon signal by using copropagating laser beams and removing the etalon from the Titanium-Sapphire laser. The pronounced feature of polarization measurement in the narrow case, decreasing polarization degree with increasing laser power, was completely eliminated.

The effects of laser power were tested by attenuation of the probe laser by factor of 10 and by attenuation of the pump laser by factor of $10^{2.4}$. With the broad two-photon signals no statistically significant effects were detected in either case.

Additional tests included the investigation of the possible density effects on the measured polarization degree. We changed the density of the sample from $2.5\times 10^{11}$ $cm^{-3}$ to $7\times10^{12}$ $cm^{-3}$ (the typical experimental density was close to $1\times10^{12}$ $cm^{-3}$). No statistically significant change in the measured $P_L$ was detected.

The effect of the finite angle between laser beams was tested by intentional increase of this angle by factor of 2 (50 mrad instead of the usual 25 mrad). This produced no statistically significant result. The effect of the shift of the observation point with respect to the sample cell was investigated by moving the photomultiplier tube off the x-axis (Fig.9) by $\pm45°$ and by changing the distance from the tube to the cell from ~5cm to ~20cm. In both cases no effect was detected.

The routine systematic tests of the polarization properties of the device, as a whole,

were performed before each set of routine runs at a given detuning by measuring the polarization degree with pump polarization direction set at $\pm 45.0°(0.1)$ to the nominal polarization direction of the probe (see Device Preparation section). No data was taken, unless the result of this test was $\pm 0.2(0.2)\%$ or better.

The rigorous tests of the Fizeau wavemeter performance were critical for this experiment. The measurement of a single line $Ar^+$ ion laser (Coherent, Model Innova-70) output yielded value $\lambda_{meas}=488.1110$ nm (all numbers correspond to vacuum), which is different from the nominal value $\lambda_{nom}=488.1225$ nm by

$$\Delta\lambda^{Ar} \equiv \lambda^{Ar}_{nom} - \lambda^{Ar}_{meas} = 0.115 \text{ Å} \tag{57}$$

with the relative error equal to

$$\frac{\Delta\lambda^{Ar}}{\lambda^{Ar}_{nom}} \simeq 2.4\times10^{-5} \tag{58}$$

The measurement of the He - Ne laser wavelength yielded value $\lambda_{meas}=632.9760$ nm which is also different from the nominal value $\lambda_{nom}=632.9914$ nm by

$$\Delta\lambda^{HeNe} \equiv \lambda^{HeNe}_{nom} - \lambda^{HeNe}_{meas} = 0.154 \text{ Å} \tag{59}$$

with the relative error

$$\frac{\Delta\lambda^{HeNe}}{\lambda^{HeNe}_{nom}} \simeq 2.4\times10^{-5} \qquad (60)$$

These relative errors are considerably larger than the quoted precision of the device ($\pm 1$ in $10^6$), but sufficiently small for a simple standard procedure of re-calibration, called a Single Point Calibration. The procedure was carried out against the $Ar^+$ ion laser single line (4881.225 Å) output. Consequently the measurement of a He - Ne laser wavelength (and, of course, the single line $Ar^+$ ion laser wavelength) gave the exact nominal values. During the experiment the periodic check of the Fizeau wavemeter performance was accomplished by measuring the wavelength of the resonant $5p^2P_{1/2} \rightarrow 8s^2S_{1/2}$ and $5p^2P_{3/2} \rightarrow 8s^2S_{1/2}$ in Rb. The typical results (in vacuum wavenumbers units) are summarized in the following table:

Table1. Comparison of the nominal and the measured resonance transitions wavenumbers.

| Resonance transition | $k_{nom} \equiv 1/\lambda_{nom}$ ($cm^{-1}$) | $k_{meas} \equiv 1/\lambda_{meas}$ ($cm^{-1}$) | $\Delta k = k_{meas} - k_{nom}$ ($cm^{-1}$) | $\Delta k/k_{nom}$ |
|---|---|---|---|---|
| $5p^2P_{1/2} \rightarrow 8s^2S_{1/2}$ | 16467.88(1) | 16467.89(2) | 0.01 | $6.1\times10^{-7}$ |
| $5p^2P_{3/2} \rightarrow 8s^2S_{1/2}$ | 16230.28(1) | 16230.29(2) | 0.01 | $6.2\times10^{-7}$ |

The typical uncertainty in polarization degree, due to deviations of the measured wavenumbers from the nominal values, is thus smaller, than $2\% \times 10^{-6}$ (see Fig.27), this value being totally negligible comparing to the typical statistical uncertainty of $P_L$ ($\pm 0.23\%$).

The birefringence of the sample cell windows was tested by inserting the cell in its normal experimental position (see Fig.9) when all polarizers and analyzers were properly aligned. A typical contrast ratio of 1/4000 was obtained in parallel and perpendicular configurations. Typically the smallest contrast ratio was 1/2000. The thermal stress of the windows was routinely reduced by a simple procedure of thermal annealing after each experimental run. We summarize the results of the systematic tests in the following table:

Table 2. The systematic effects budget.

| Parameter | Lasers power | Sample density | Beams divergency | Counting nonlinearity | Observation geometry |
|---|---|---|---|---|---|
| $\Delta P_L$ (%) | 0.02 | 0.003 | 0.01 | 0.02 | 0.017 |

The net average uncertainty of the measured $P_L$, due to average counting statistics uncertainty (0.23%) and all factors listed in the table, combined in quadrature is 0.233%.

# V. Results

The result of our experiment is a polarization spectrum of the atomic rubidium, obtained in the range of detunings from - 417 $cm^{-1}$ to +99 $cm^{-1}$. The spectrum is represented by 105 experimental points, polarization degree vs. detuning (Fig.27), gathered in 23 groups. In each group the detunings, corresponding to individual points, are close to each other in detunings (the typical differences are ~0.05 $cm^{-1}$), and therefore the experimental points from one group are almost indistinguishable on the graph. The average uncertainty of any single measured polarization degree is $\pm 0.233\%$, which is almost entirely due to the statistical uncertainty of numbers of photons. The average uncertainty of the measured detuning is $\pm 0.02$ $cm^{-1}$. Such error bars are too small to be seen on the scale of the Fig.27.

The solid curve on Fig.27 is a fit to the data, using the theoretical polarization shape, defined by Eq.(39),(40) and Eq.(35). It corresponds to the following set of parameters: $R = 1.013$, $p = -6\times10^{-5}$ cm, and $q = 2\times10^{-6}$ cm. The plot of the corresponding residuals ( defined as a difference of the measured and the theoretical polarization degree) is shown in Fig.28. The solid horizontal line at -0.017% shows the average residual. Two other horizontal lines indicate a standard deviation of 0.20%. The fitting

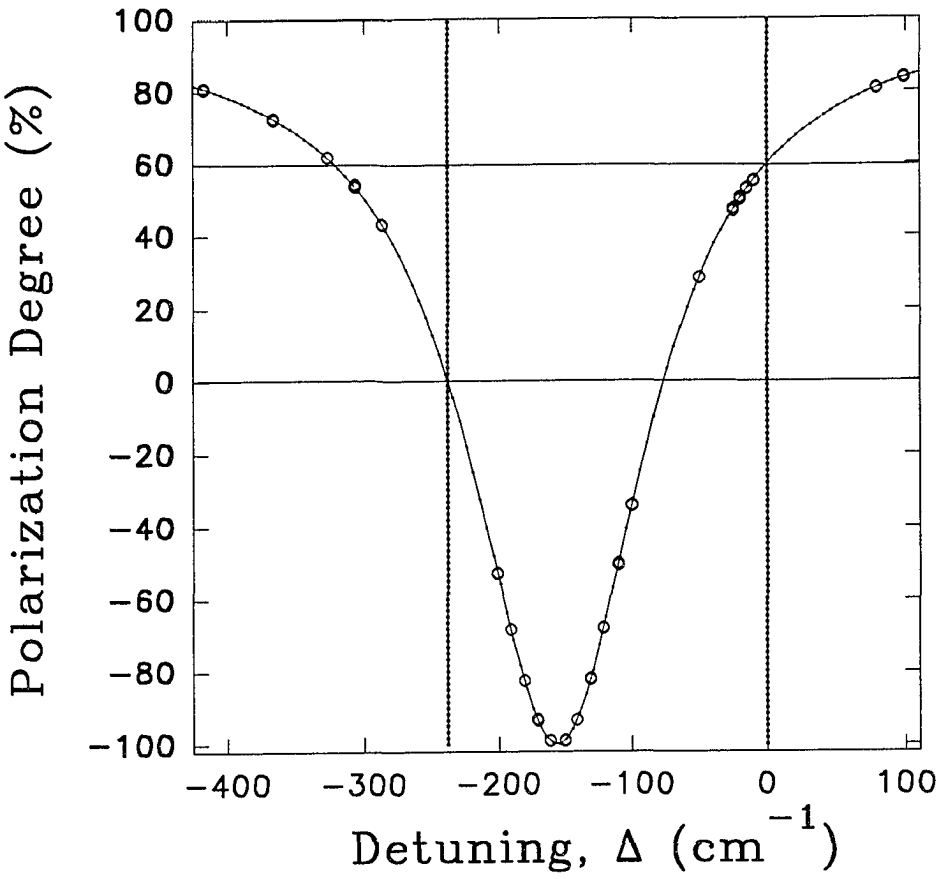


Figure 27. Experimental (circles) and theoretical (solid curve) polarization degree versus detuning.

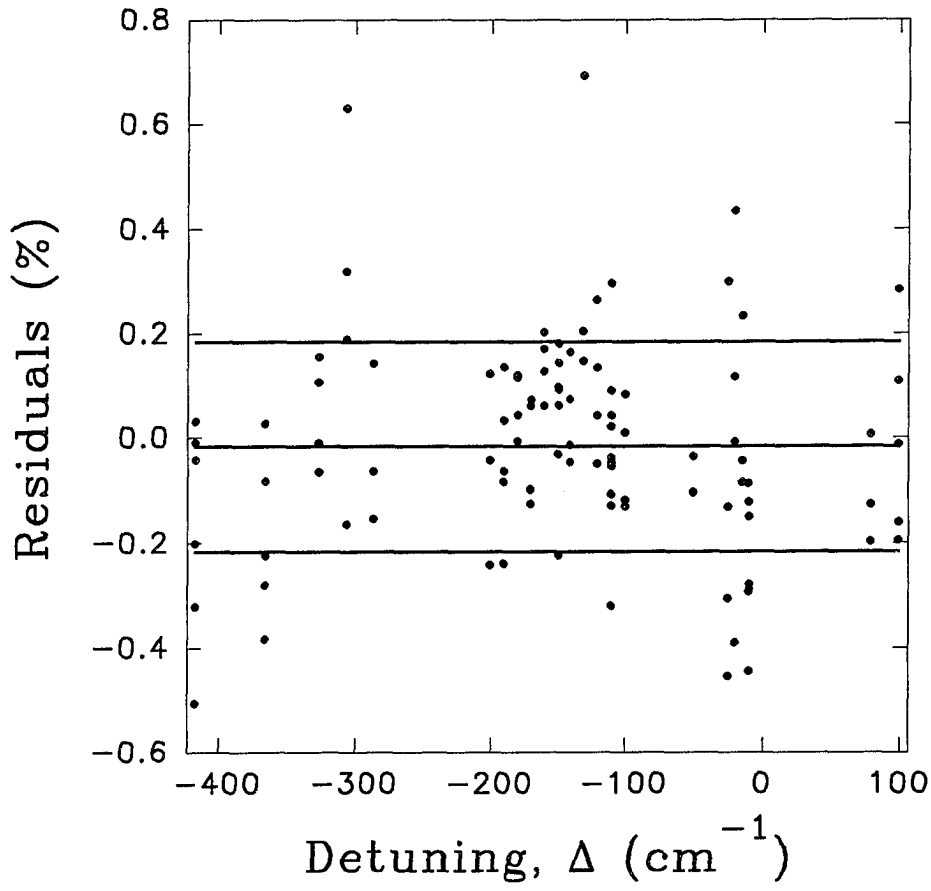


Figure 28. Plot of the residuals.

procedure was carried out in a 3 - dimensional free parameter space,{ $R$, $p$ and $q$}, and was based on an algorithm, described in [70]. The minimum of the $\chi^2$, equal to approximately 77, defined the parameter $q$ uniquely. (Recall, that number of the experimental points is 105, so the number of the degree of freedom is 102). The two other parameters, $R$ and $p$, can be varied over a wide range of values, without changing $\chi^2$ significantly. The variations of $R$ and $p$ consistent with minimum $\chi^2$ are not independent, as any value of $R$ yields a unique value of $p$ and vice versa. In the process of the fitting it became evident that the values of $R$ and $p$, initially considered independent, are strongly correlated. Several attempts to avoid correlation, by forming some different then $P_L$ functions of the experimental data ($N_\parallel$ and $N_\perp$) and fitting to them the corresponding theoretical functions, led rapidly to the realization that separate determination of $R$ and $p$ requires an experimental precision several orders of magnitude better than that obtained - a totally unrealistic requirement at the present time. We realized that the correlation of $R$ and $p$, defined at the current level of precision of our experiment, represents by itself an extraordinarily exact and valuable piece of information about atomic rubidium.

The nature of the correlation can be best understood when one considers the global features of the theoretical polarization degree curve. For $R > 0$ in the considered region of detunings, the $P_L(\Delta)$ curve has one minimum ($P_L$=-100%) at some detuning, located between 0 and -237.60 $cm^{-1}$ (for $R$ close to 1 and $p$ close to zero this detuning

is close to -158.4 $cm^{-1}$ which is 2/3 of the fine structure splitting). We will refer to this minima as a critical point $\omega_{c1}$. The two other important points, namely $\Delta = 0$ $cm^{-1}$ , $P_L(\Delta) = 60$ %, and $\Delta$ =-237.60 $cm^{-1}$ , $P_L(\Delta) = 0$ % are to a very high level of precision independent of the values of *R*, *p* and *q*, as one can see from Eq.(39),(40), and(35). These points we will call the critical points $\omega_{c2}$ and $\omega_{c3}$ respectively. The weak-field radiative properties of the system under consideration define only the position of the critical point $\omega_{c1}$, but the positions of $\omega_{c2}$ and $\omega_{c3}$ are independent of them. What is affected by these properties, except for the exact position of $\omega_{c1}$, are fine details of the curvature of the curve $P_L(\Delta)$ between and outside the critical points. These, however, are so small that it would require an experimental precision, several orders of magnitude better than ours to extract *R* and *p* separately from the direct experimental data. Although such precision is possible in principle, from a practical point of view one has to consider the actually obtained information, in the form of the correlation of *R* and *p*, as an experimental state-of-the-art outcome of this experiment. When this was realized, in order to test this point of view, the fitting procedure was changed: instead of considering *R* and *p* as independent parameters, they were related through the equation

$$P_L(\omega_{c_1}) = - 100\ \% \qquad \textbf{(61)}$$

which defines the location of $\omega_{c1}$. Then in the fitting procedure the parameters *R*, $\omega_{c1}$,

and $q$ were taken as the independent parameters. The fitting procedure yielded a **unique** value of

$$\omega_{c_1} = -155.82\ cm^{-1} \pm 0.03\ cm^{-1} \qquad (62)$$

where the uncertainty corresponds to an increase of $\chi^2$ by 1 from its minimum value. The value of $R$ again can be varied in a wide range, without changing $\chi^2$. Substitution of Eq.(62) into Eq.(61) yields a linear relation between $R$ and $p$, almost identical with the one deduced from the correlation of $R$ and $p$ when they were treated as independent parameters in the fitting procedure:

$$R = 1.01756\ (57) + 81.466\ (15)\ p \qquad (63)$$

where $p$ is in units of cm and $R$ is dimensionless. We accept this as a confirmation of the idea, that the position of the critical point $\omega_{c1}$ dominates the entire experimental spectra in the investigated region. Eq.(61) with precisely defined $\omega_{c1}$, Eq.(62), presents a global characteristic of the radiative properties of the studied system. It relates the relative size of the electric dipole matrix elements between initial, final and the main intermediate states on one side, to these, contributed to the two-photon absorption process, by the higher excited intermediate states, on the other. This kind of a global information can be compared to the case, when the lifetime of a highly excited state of an atom is known and several channels of decay are possible. What is different in this

case is that, unlike the lifetime case where the often compatible branching ratios completely blend information about separate transition probabilities, the modest precision in estimation of the contribution of the higher excited intermediate states, when it is small, will yield a high precision result for the main intermediate state. When the contribution of the higher excited intermediate states is estimated as not too small, then the requirements for precision of estimation became more severe.

Let us examine the precision with which $R$ can be obtained from our results. We want to obtain an order-of-magnitude estimation of $p$, so the results of relatively simple calculations based on the Coulomb approximation (fine structure is ignored) [71] will be sufficiently accurate. The absolute values of the required ratios of the reduced matrix elements, obtained from these calculations, are summarized in the following table (the contributions of the intermediate nP-levels, with n higher then 10 are neglected, which is justified in this estimation):

Table 3. Ratios of the radial matrix elemens products.

$$S_n \equiv [\langle 8s\|r\|np\rangle \langle np\|r\|5s\rangle] \times [\langle 8s\|r\|5p\rangle \langle 5p\|r\|5s\rangle]^{-1}, \quad n=6\text{-}10.$$

| $S_6$ | $S_7$ | $S_8$ | $S_9$ | $S_{10}$ |
|---|---|---|---|---|
| 0.456 | 1.831 | 1.750 | 0.153 | 0.049 |

The summation of the corresponding contributions to $p$, with no possible cancellations considered, give $p \sim -10^{-3}$ cm. Note, that the absolute value of this estimation is probably too high, as all of the contributions to $p$ will likely not have the same sign. Let us assume that $p$ is more rigorously estimated to be $-10^{-3}$ cm with the uncertainty of 10%, i.e.

$$p = -1\times10^{-3} \quad ( 10^{-4} ) \ (cm) \tag{64}$$

Substituting this into eq.(63) yields

$$R = 0.9361 \pm 0.0088 \tag{65}$$

Thus the relative precision for $R$ is on the order of 1% - 10 times better, than that of $p$. If the value of $p$, found in a more careful theoretical estimation, would be on the order of ($-10^{-4}$ cm ), with the same precision of 10%, the precision of $r$ would become 0.1%.

The obtained spectra also indicates that the parameter $R$ has a positive value. For negative $R$ the maximum of $P_L$ at +100% would have been observed at some detuning between 0 $cm^{-1}$ and -237.60 $cm^{-1}$. In other words, there is no detuning in the considered spectral region where $I_\perp=0$. This fact is manifested in the fitting procedure as well: there is no correlation between $R$ and $q$ ; q has a unique value

$$q = 2 \times 10^{-6} \ (5) \ (cm) \tag{66}$$

This quantity represents information about the combined effect of the relativistic and many particle corrections to the hydrogenic wavefunction of a family of levels of the rubidium atom involved in the studied process of the two-photon absorption. The relation of $R$ and $p$ and the $q$ value itself, can be considered as a specific, experimentally established sum rules and serve as a test for the validity of the theoretical wavefunctions.

# VI. Conclusions

As a result of the measured two-photon polarization spectra, the precise relation of parameters of the rubidium atomic structure, $R$ and $p$ was established (Eq.63) and a unique value of the parameter $q$ was obtained (Eq.66). These parameters characterize the combined effect of the relativistic and many body corrections to the initial, final, and the principal intermediate states wavefunctions of rubidium ( $R$ parameter), and those due to the more energetic intermediate states ( $p$ and $q$ parameters) involved in the investigated two-photon absorption. The obtained results can be used as a benchmark for testing the accuracy of theoretical wavefunctions.

From the experimental point of view, this investigation, as well as that carried out previously [72], show that the technique of two-photon, two-color polarization

spectroscopy is a powerful tool for obtaining precise information about the radiative properties of the atoms. Some features of this technique, namely the easily achievable low background level, insensitivity to drift of the laser power, frequency and naturally avoided single photon resonances, make it much better than some traditional spectroscopic techniques.

This technique can be properly modified for use in Rayleigh scattering experiments, and the possibility of this is being considered. In the described experiment the main intermediate levels of the process are represented by the fine structure components of Rb : $5p^2P_{1/2}$ and $5p^2P_{3/2}$. With the appropriate choice of the sample and laser frequencies, different orbital wavefunctions can be selected for this purpose, for example the S and D orbitals in P→{S;D}→P transitions or nP (n±1)P in S→{nP;(n±1)P}→{S or D} transitions. In such experiments the properties of the involved orbitals can be compared with each other in a manner similar to that presented in this work and new useful and precise information about the atomic structure can be revealed.

# BIBLIOGRAPHY


1. A.S. Zibrov, M.D. Lukin, D.E. Nikonov, L. Hollberg, M.O. Scully, V.L. Velichansky, and H.G. Robinson, Phys. Rev. Lett. 75 , 1499 (1995).
2. G.E. Stedman, in *Modern Nonlinear Optics*, edited by M. Evans and S. Kielich (Willey, 1993), Part 2; C.E. Tanner, in *AIP Conference Proceedings, 323*, edited by D.J. Wineland, C.E. Wieman and S.J. Smith (AIP Press,1994); S.L. Gilbert, M.C. Noecker, R.N. Watts, and C.E. Wieman, Rhys. Rev. Lett. 55 , 2680 (1985); D.M. Meekhof, P.A. Vetter, P.K. Majumder, S.K. Lamoreaux, and E.N. Fortson, Phys. Rev. A52,1895 (1995).
3. *Atomic and Molecular Data for Space Astronomy. Needs, Analysis, and Availability. Lecture Notes in Physics, 407*, edited by P.L. Smith and W.L. Wiese (Springer, Berlin, 1991).
4. A. Einstein. On the Quantum Theory of Radiation, in *Sources of Quantum Mechanics*, edited by B.L. van der Waerden (Dover, 1967).
5. *Sources of Quantum Mechanics*, edited by B.L. van der Waerden (Dover, 1967).
6. A. Corney, *Atomic and Laser Spectroscopy* (Clarendon Press, 1988).
7. H.A. Bethe and E.E. Salpeter, *Quantum Mechanics of One- and Two - Electron Atoms* (Plenum, 1977).
8. I.I. Sobelman, *Atomic Spectra and Radiative Transitions* (Springer, Berlin, 1991).
9 . W.L. Wiese, in *Progress in Atomic Spectroscopy*, edited by W. Hanle and

H. Kleinpoppen (Plenum, New York,1978), Part B.

10. M.C.E. Huber, R.J. Sandeman, Phys. Scripta 22, 373 ( 1980).
11. U. Fano, J.W. Cooper, Rev. Mod. Phys. 40, 441 (1968).
12. C. Cohen-Tannoudji, B. Diu, and F. Laloë, *Quantum Mechanics* (Wiley, 1977), Vol.II.
13. E.U. Condon and G.H. Shortley, *The Theory of Atomic Spectra* ( Cambridge, 1991).
14. M. Mizushima, *Quantum Mechanics of Atomic Spectra and Atomic Structure* (Benjamin,1970).
15. J. Carlsson, Phys. Scripta 39, 442 (1989).
16. J.K. Link, J. Op. Soc. Am. 56, 1195 (1966).
17. E.A. Bailey and G.K. Rollefson, J. Chem. Phys. 21, 1315 (1953).
18. W. Hanle, Z. Physik 30, 93 (1924).
19. F.D. Colgrove, P.A. Franken, R.R. Lewis, and R.H. Sands, Phys. Rev. Lett. 3, 420 (1959).
20. G. Breit, Rev. Mod. Phys. 5, 91 (1933).
21. Al.I. Lupascu, I.M. Popescu, and St. Tudorache, Rev. Roum. Phys. 22, 923 (1977).
22. M.A. Rebolledo and J.J. Sanz, Phys. Rev. A 29, 1938 (1984).
23. A. Gallagher and E.L. Lewis, Phys. Rev. A10, 231 (1974).
24. E.L. Altman and S.A. Kazantsev, Opt. Spectr. 28, 432 (1970).
25. G. Belin and S. Svanberg, Phys. Scripta 4, 269 (1971).
26. R. W. Schmiedler, A. Lurio, W. Happer and A. Khadjavi, Phys. Rev. A2, 1216 (1970).

27. J. Marek and P. Muenster, J. Phys. B13, 1731 (1980).

28. G. Waligorski, P. Kowalczyk, and C. Radzewicz, Z. Phys. D3, 79 (1986).

29. C.H. Greene and R.N. Zare, Annu. Rev. Phys. Chem. 33,119 (1982).

30. D.S. Rozhdestvenskii, Ann. Physik (Leipzig) 39, 307 (1912).

31. S. Svanberg, *Atomic and Molecular Spectroscopy* (Spinger,1992).

32. S.S. Zeilikovich, V.A. Komarovskii, S.A. Pulkin, and L.S. Gaida, Opt. Spectrosc. 57, 486 (1984).

33. L.N. Shabanova and A.N. Khlystalov, Opt. Spectrosc. 56, 128 (1984).

34. D. von der Goltz, W. Hansen, and J. Richter, Phys. Scripta 30, 244 (1984).

35. E. Caliebe and K. Niemax, J. Phys. B 12, L45 (1979).

36. M.L. Pascu, T.M. Dang and G. Dumbraveanu, Rev. Roum. Phys 27, 659 (1982).

37. H. Puell, C.R. Vidal, Opt. Commun 19, 279 (1976).

38. M. Schubert and B. Wilhelmi, *Nonlinear Optics and Quantum Electronics* (Wiley, 1986).

39. W.A. van Wijngaarden, K.Bonin, W. Happer, E. Miron, D. Schreiber, and T. Arisawa, Phys. Rev. Lett. 56, 2024 (1986).

40. W.A. van Wijngaarden, K.D. Bonin, and W. Happer, Hyperfine Interactions 38, 471 (1987).

41. L.I. Schiff, *Quantum Mechanics*, Third Edition (McGraw-Hill, 1968).

42. A. Gold, in *E. Fermi Course 42*, edited by R.J. Glauber (Academic Press, 1969).

43. M. Göppert - Mayer, Naturwissenschaften 17, 932 (1929).

44. J.D. Jackson, *Classical Electrodynamics* (Wiley, 1975).

45. H. Goldstein, *Classical Mechanics* (Addison-Wesley, 1981).

46. J.J. Sakurai, *Advanced Quantum Mechanics* (Addison-Wesley, 1984).

47. M. Weissbluth, *Atoms and Molecules* (Academic Press, 1978).

48. R.W. Boyd, *Nonlinear Optics* (Academic Press,1992).

49. M. Havey, private communication.

50. G. Arfken, *Mathematical Methods for Physicists* (Academic Press,1985).

51. M.E. Rose, *Elementary Theory of Angular Momentum* (Wiley, 1957).

52. G.K. Woodgate, *Elementary Atomic Structure* (Oxford, 1989).

53. A.S. Davydov, *Quantum Mechanics* (Pergamon, 1976).

54. B.N. Chichkov and V.P. Shevelko, Phys. Scripta 23,1055 (1981).

55. P.I. Gruzdev and V.I. Denisov, Opt. Spectrosc. 52, 8 (1982).

56. S.R. Langhoff, C.W. Bauschlicher, and Jr., H. Partridge, J.Phys. B 18, 13 (1985).

57. J. Migdalek and E. Banasinska, J.Quant. Spectrosc. Radiat. Transfer 48, 341 (1992).

58. N. Bloembergen and M.D. Levenson, in *High - resolution Laser Spectroscopy*, edited by K. Shimoda (Springer, 1976).

59. R.F. Bacher, and S. Goudsmit, *Atomic energy states* (Greenwood Press,1968).

60. T.F. Gallagher, *Rydberg Atoms* (Cambridge, 1994).

61. B.S. Mathur, H. Tang, and W. Happer, Phys.Rev. 171, 11 (1968).

62. D.R. Lide, *CRC Handbook of Chemistry and Physics* (CRC Press,1995).

63. H.M. Gibbs, G.C. Churchill, J. Opt. Soc. Am. 62,1130 (1972).

64. E. Arimondo, M. Inguscio, and P.Violino, Rev. Mod. Phys. 49, 31 (1977).

65. D.E. Roberts and E.N. Fortson, Opt. Comm. 14, 332 (1975).

66. a) The result for $^{87}Rb$ obtained independently by author and Dr. M. Havey (private communication) using different schemes of calculation. The form of the presentation of the results, Fig.2 , is due to Dr. M. Havey. See also C. Cohen - Tannoudji and Kastler, in *Progress in Optics*, edited by E.Wolf ( Wiley, 1965), Volume V.

b) M. Havey, private communication.

67. G. Grynberg, B. Cagnac, and F. Biraben, in *Incoherent Nonlinear Optics*, edited by M.S. Feld, and V.S. Letochov (Springer, 1980).

68. J. Hoffnagle, Opt. Comm. 42, 267 (1982).

69. W. Happer, Rev. Mod. Phys. 44,169 (1972).

70. P.R. Bevington and D.K. Robinson, *Data Reduction and Error Analysis For the Physical Sciences* (McGraw - Hill, 1992).

71. A. Lindgård and S.E. Nielsen , Atomic Data and Nuclear Data Tables, Academic Press, 19, p.606 (1977).

72. R.P. Meyer. Precision Measurement of Relative Dipole Matrix Elements in Atomic Sodium. Dissertation, Old Dominion University (1995).

# BIOGRAPHY

Alexander I. Beger was born in Samgorodok, Ukraine (former USSR) on November 18, 1956. He graduated from Samgorodok secondary school in 1973 and continued his education at Tartu State University, Tartu, Estonia (former USSR). He graduated from Tartu State University in 1978 with a Diploma in physics . He made first attempt to emigrate from USSR in 1980, when the emigration was almost completely stopped. After emigration with his family to United States in 1990, Alexander I. Beger continued his studies in physics at Old Dominion University as a graduate student. He received M. S. degree in physics in 1992. He is a member of the American Physics Honor Society ($\Sigma\Pi\Sigma$) and the American Physics Society.